Comunicações Geológicas

Comunicações Geológicas (2023) 110, 1, 7-23
ISSN: 0873-948X; **e-ISSN:** 1647-581X

The Bemposta Migmatite Complex (Central-Iberian Zone, NE Portugal): a petrographic and geochemical study

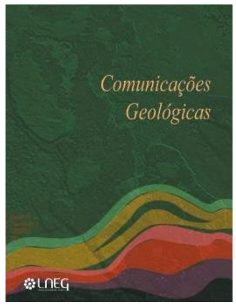

Petrografia e Geoquímica do Complexo Migmatítico de Bemposta (Zona Centro Ibérica, NE de Portugal)

F. Martins[1,3], A. Damas[1], M. R. Azevedo[1], M. E. Gomes[2*], B. V. Aguado[1], J. A. Nogueira Neto[3]

DOI: https://doi.org/10.34637/qd2z-my62

Recebido em 02/02/2022 / Aceite em 25/02/2023

Publicado online em maio de 2023

Artigo original
Original article

Abstract: The Bemposta Migmatite Complex (CMB) belong to the Central-Iberian Zone, NE Portugal. It is a high-grade metamorphic belt composed by metasediments of Ediacarian-Lower Cambrian age affected by partial melting during the second Variscan deformation event (D_2). The anatexis culminated with intrusion of syn-tardi-D_2 leucogranite sills in the CMB. Field and petrographic evidence suggest that the anatexis of the metasediments was controlled by muscovite dehydration-melting reactions. On the other hand, the stromatic leucosomes show that they were probably produced at a slightly deeper structural level (through biotite dehydration-melting reactions) and subsequently injected in these lithologies. The geochemical data reveals that leucosomes no longer correspond to the original melt compositions. During melt migration and ascent, they underwent fractional crystallization and accumulation of K-feldspar. Syn-tardi-D_2 leucogranites that intrude CMB were most likely produced by higher degrees of partial melting. They have fractionated compositions and variable degrees of contamination with residual accessory mineral phases. Thus, CMB is interpreted as a Migmatite Injection Complex, where anatectic melts produced at slightly deeper levels were accumulated.

Keywords: Bemposta Migmatitic Complex, anatexis, syn-tardi-D_2 leucogranites, Migmatitic Injection Complex.

Resumo: O Complexo Migmatítico de Bemposta (CMB) situa-se na Zona Centro Ibérica (NE Portugal) correspondendo a um cinturão metamórfico de alto grau, composto por metassedimentos do Ediacariano-Câmbrico Inferior afetados por fusão parcial durante a segunda fase de deformação Varisca (D_2). A anatexia destas rochas culminou com a intrusão de leucogranitos sin-tardi-D_2 do tipo *sill*. As evidências de campo em consonância com a petrografia sugerem que a anatexia dos metassedimentos foi controlada pela reação de desidratação da moscovite. Os leucossomas mostram evidências de terem sido produzidos em níveis estruturais inferiores (através da reação da desidratação da biotite) e subsequentemente injetados nestas litologias. Os dados de geoquímica revelam que os leucossomas durante a sua ascensão foram afetados por cristalização fracionada e acumulação de feldspato potássico. Os leucogranitos sin-tardi-D_2 que intruem o CMB resultaram de altas taxas de fusão e possuem composições equivalentes a magmas afetados por cristalização fracionada, contaminados por minerais acessórios residuais. Assim, o CMB é interpretado como um Complexo Migmatítico de Injeção, onde os líquidos anatéticos produzidos em profundidade se acumularam.

Palavras-chave: Complexo Migmatítico de Bemposta, anatexia, leucogranitos sin-tardi-D_2, Complexo Migmatítico de Injeção.

[1] Universidade de Aveiro, Departamento de Geociências, GEOBIOTEC, Aveiro, Portugal.
[2] Universidade de Trás-os-Montes e Alto Douro, ECVA, Pólo Centro de Geociências, Vila Real Portugal.
[3] Universidade Federal do Ceará, Departamento de Geologia, Fortaleza, Ceará, Brasil.

* Corresponding author / Autor correspondente: mgomes@utad.pt

1. Introduction

The study of exposed migmatitic terranes is a unique opportunity to understand the tectonic-metamorphic processes associated with the generation of granitic magmas in deep zones of the continental crust during mountain building. A careful and comprehensive study of the metamorphic and deformation processes overprinted in the migmatitic rocks and associated leucogranites aid to understand the evolved mechanisms, in these deep levels of the crust.

At the Bemposta region, located in the northern Portugal, outcrops a variscan migmatite complex, known as Bemposta Migmatite Complex (BMC). BMC represents a segment of the Iberian Variscan Belt, belong to the Central-Iberian Zone (ZIC), NE Portugal, where stands out the presence of pelite-derived stromatic migmatites, minor boddies of orthogneisses and variscan leucogranites.

In this paper, we present the new petrographic and geochemical data for metasediments, migmatites and leucogranites exposed in Bemposta Migmatite Complex (NE Portugal) in order to evaluate the genetic relationship between them, and consequently understand the partial melting processes and generation of granitic magmas which took place in this sector of the Variscan Belt.

2. Geological setting

The region of Bemposta is located in the NW sector of the Iberian Massif, between latitudes 41°23’40’’N-41°14’30’’N and longitudes 6°42’00’’W-6°23’00’’W (Fig. 1). The Iberian Massif represents the westernmost segment of the European Variscan

Belt, formed during the collision between Gondwana and Laurentia that culminated with formation of the super-continent Pangea, in the final of the Paleozoic (Ribeiro *et al*., 2007; Dias *et al*., 2016). This sector of the Variscan Belt has been divided in 6 zones, according to different geological characteristics (Arenas *et al*., 1986; Ribeiro *et al*., 2007). These are, from NE to SW: Cantabrian Zone (CZ); West Asturian Leonese Zone (WALZ); Central Iberian Zone (CIZ); Galiza Trás-os-Montes Zone (GTMZ); Ossa-Morena Zone (OMZ) and South Portuguese Zone (SPZ).

The studied area is located in the CIZ and to the northwest it is bordered by the parautochthonous and allochthonous terranes of the GTMZ (Fig. 1a).

CIZ is interpreted as an internal zone of the Iberian Massif, characterized by the presence of some high-grade metamorphic complexes of regional extent and granitic magmatism Experimental Constraints on Hercynian Anatexis in the Iberian Massif, Spain (Castro *et al*, 2000,) The architecture present in CIZ terranes is consequence of three deformation phases, which acted during Variscan Orogeny (*e.g.* Noronha *et al*., 1981; Díez Balda *et al*., 1990; Ribeiro *et al*., 1990; Dias and Ribeiro, 1995; Valle Aguado *et al*., 2005; Martínez Catalán *et al*., 2004, 2007; Dias *et al*., 2006, 2013, 2016).

The D_1 deformation phase, related to the crustal thickening stage, was compressive and induced a Barrovian-type prograde metamorphism in the CIZ domain. The D_1 structures were variably overprinted by D_2 extensional deformation phase attributed to a large-scale gravitational collapse of the thickened continental crust (*e.g.* Arenas and Catalán, 2003; Escuder Viruete *et al*., 1994; Martínez Catalán *et al*., 2009; Valle Aguado *et al*., 2005). At this deformation stage, it was achieved the metamorphic peak conditions and consequently were formed metamorphic domes, which was accompanied by the formation of migmatitic complexes at deep structural levels. And lastly, a D_3 deformation phase which related to strike-slip, sinistral and dextral, subvertical shear zones, in the final stages of Variscan Orogeny (Martínez Catalán *et al*., 2009). During D_3, the metamorphism has developed under retrograde conditions achieving greenschist facies at high crustal levels, whilst in lower crustal levels, high temperatures could have locally persisted as a result of the high thermal gradients inherited from D_2 and the intrusion of syn-D_3 granitoids.

3. The Bemposta Migmatite Complex

The Bemposta Migmatite Complex, observed in figure 1b, constitutes a high-grade metamorphic belt aligned according to NE-SW trend, outcropping along the Douro River canyon, between Bemposta (NE Portugal) and Fermoselle (Spain). It is mainly composed by Ediacarian-Lower Cambrian metasediments from Douro Group, intensely migmatized during the Variscan

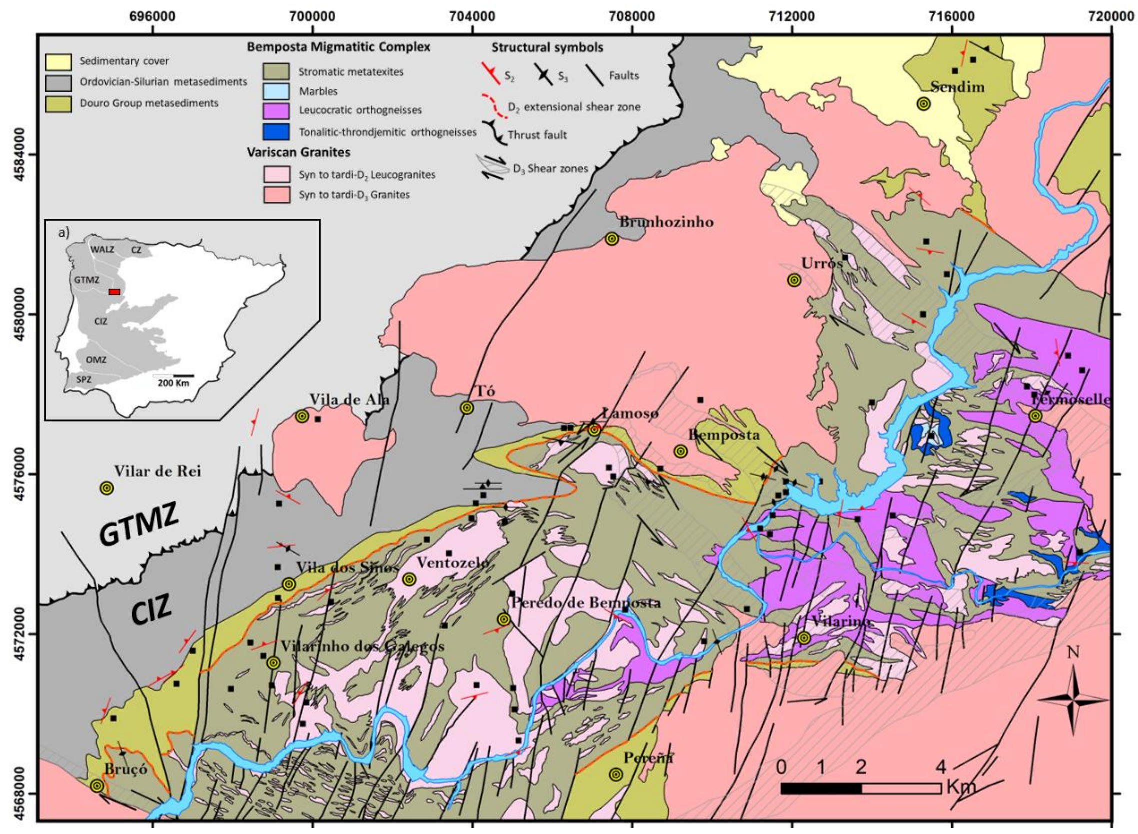

Figure 1. (a) Iberian Massif and their subdivision in six zones, showing the location of the study area (red square). CZ: Cantabrian Zone; WALZ: West Asturian Leonese Zone; CIZ: Central Iberian Zone; ZGTM: Galiza Trás-os-Montes Zone; OMZ: Ossa-Morena Zone; SPZ: South Portuguese Zone. (b) Geological map of the Bemposta Migmatitic Complex limited by D_2- extensional shear zone. Samples location are plotted with black squares (Modified from Lazuen Alcón *et al.* (1981), Sanz Santos *et al.* (2000a, b), Pereira *et al.* (2001) and Dias da Silva (2013).

Figura 1. (a) Localização da área de estudo (polígono vermelho) no Maciço Ibérico. CZ: Zona Cantábrica; WALZ: Zona Asturo-Leonesa; CIZ: Zona Centro Ibérica; ZGTM: Zona Galiza-Trás-os-Montes; OMZ: Zona Ossa-Morena; SPZ: Zona Sul Portuguesa. (b) Mapa Geológico do Complexo Migmatítico de Bemposta, limitado pela zona de cisalhamento extensional D_2 (modificado de Lazuen Alcón *et al.* (1981), Sanz Santos *et al.* (2000a, b), Pereira *et al.* (2001) e Dias da Silva (2013).

Orogeny (Escuder Viruete *et al*., 1994, 1997, 1998, 2000; Pereira *et al*., 2006; Dias da Silva, 2013). Particularly in the Spanish part of the study area, the migmatitic metasediments are interspersed with lenticular bodies of orthogneisses. These ortho-derived rocks are leucocratic, display "augen" textures or gneissic banded textures and, in some areas, they also appear migmatized. On the other hand, migmatites where neosomes predominate, and which show a greater degree of partial melting (almost complete melting), are classified as diatexites. Diatexites may include "schlieren" that represent aggregates of mafic minerals with preferential orientation, generally parallel to the syn-anatexis flow. The "schlieren" are thin and generally discontinuous bands, consisting of an aggregate of mafic minerals (biotite, sillimanite, pyroxene and also plagioclase). Geochronological studies (U/Pb on zircon) in similar orthogneisses from Miranda do Douro and orthogneisses from Fermoselle provided a crystallization ages interval between 480 and 499 Ma, indicating a Cambro-ordovician age for their magmatic precursors (Bea *et al*., 2006; Zeck *et al*., 2007; Talavera *et al*., 2013).

The BMC contacts with a narrow strip of non-migmatized metasediments from Douro Group or, in some places, by Ordovician-Silurian metasediments. The contact between them corresponds to a major extensional shear zone which acted during D_2 variscan deformation phase, related with a large-scale gravitational collapse of the thickened continental crust (Escuder Viruete *et al*., 1994, 1997, 1998, 2000).

At outcrop scale, the migmatitic metasediments are characterized by a horizontal stromatic banded, marked by an alternation between quartz-feldspathic bands (leucosomes) and dark biotite-sillimanite-rich layers (mesosomes) (Fig. 2a). According to Sawyer (2008), the regular alternation between leucosomes and mesosomes observed in migmatites permits to classify as *stromatic metatexites*. The leucossomes bands (thickness ranges from centimetric to decimetric) are according with S_2 mesosome foliation, suggest that the stromatic banded was generated during D_2 extensional event (Fig. 2b). The stromatic metatexites often appear affected by D_3, producing open folds with vertical axial planes and NW-SE axis. During D_3, also act a strike-slip sub-vertical shear zones that may be responsible for the verticalization of the S_2 stromatic bands (*e.g.* Dias da Silva, 2013). Due to the D_2 fabric intensity, D_1 structures are not recognizable at mesoscopic scale.

The stromatic metatexites outcrops usually enclose competent discontinuous layers of calc-silicate and metapsamitic rocks, which are considered resistant phases to partial melting processes (Fig. 2c). Despite the massive aspect, these rocks accompanied the D_2 structures and may appear weakly foliated.

The study area was intensely intruded by variscan granites that are grouped in two types. The first group corresponds to syn-tardi-D_2 leucogranites sills that can be diatextites occur associated with BMC (Fig. 2d). They are medium to coarse-grained and sometimes exhibit centimetre-sized metasediment enclaves (Figs. 2e, f). The second group, composed by syn-tardi-D_3 granites, occur mainly associated with country rocks of the BMC and appear to describe discordant relations with D_2.

4. Analytical Methods

Representative samples from Bemposta rocks were selected for whole-rock geochemistry analysis. In case of the migmatitic rocks, care was taken in separate the mesosome from the leucosome. After this, the rock samples were crushed and milled, until to obtain a powder. The analysis were carried out by Activation Laboratories- Actlabs (Ontario, Canadá), using the analytic package designated by *4LITHORESEARCH*. Major elements were analysed by IPC-AES (Inductively Coupled Plasma Atomic Emission Spectrometry), whereas trace elements were analysed by ICP-MS (Inductively Coupled Plasma Mass Spectrometry). The major and trace element compositions are given in supplementary tables 1 and 2.

Representative samples from BMC rocks were selected for microprobe analyses at the Electron Probe Microanalyser Laboratory in University of São Paulo (USP). Chemical analyses were performed on plagioclase, K-feldspar, biotite and garnet with respective mineral chemistry data given in table 1.

5. Petrography and mineral chemistry

The petrographic study comprises the analysis of metasedimentary rocks from Douro Group, BMC stromatic metatexites and associated syn-tardi-D_2 leucogranites. The Douro Group metasedimentary rocks have pelitic-greywacke composition and their main mineral assemblage is composed by biotite (Bt), muscovite (Ms), quartz (Qtz), plagioclase (Pl), ± staurolite (St), ± sillimanite (Sil) ± andalusite (And) ± cordierite (Crd), ± tourmaline (Tur). The most common accessory mineral phases are the zircon (Zrn), monazite (Mnz), apatite (Ap), rutile (Rt) and opaque minerals. Their textures are lepidogranoblastic or lepidogranoporphyroblastic. Based on identified mineralogy, the metamorphic zoning along the metassediments of Douro Group vary in a short extension from biotite-zone to sillimanite-zone.

The main foliation of these rocks, defined by phyllosilicates, is sub-horizontal and corresponds to S_2 (Fig. 3a). The S_2 planes go around pre-kinematic poikiloblasts of biotite with discordant inclusion trails, which is an evidence of a previous foliation (S_1) (Fig. 3b). Despite this evidence, it is very difficult to establish the evolution of these rocks during D_1, because D_2 was very intense and erased the previous mineral paragenesis. Sillimanite corresponds to the fibrous variety and is aligned with S_2-lepidoblastic domains, which seems to indicate that the sillimanite zone was attained during D_2.

S_2 may appear affected by D_3 folds (Fig. 3c) and, in some cases, near to strike-slip sub-vertical shear zones, a S_3 mylonitic foliation is developed. The andalusite poikiloblasts may include biotite, sillimanite and staurolite, showing textural evidence that are post-S_2, and suggest that their blastesis occurred in retrograde metamorphic trend, during D_3 (Fig. 3d). Furthermore, andalusite usually erases the previous paragenesis and prevent understanding the metamorphic evolution. The cordierite poikiloblasts often contains inclusions of sillimanite and also shows evidences that it grew during retrograde metamorphic trend or any contact metamorphism could be occur.

The stromatic metatexites have mesosomes with lepidogranoblastic textures, defined by the alternance of millimetre-thick biotite-sillimanite-rich and highly recrystallized quartz-feldspar layers (Fig. 4a). Mesosomes also may have muscovite and andalusite. Muscovites has textural evidences for being secondary, which demonstrate that it grew during D_3. Andalusite was observed in some mesosomes and has the same characteristics to those of Douro Group metasediments. The garnet was never observed in the mesosome domains. The accessory phases are tourmaline, zircon, monazite, apatite and rutile.

Table 1. Chemical analyses (oxides in wt. % and trace elements in ppm) of Douro Group, mesosomes, leucosomes and leucogranites.

Tabela 1. Composição química das amostras do Grupo do Douro, mesossomas, leucossomas e leucogranitos.

	Douro Group								***Mesosomes***										
	FD1	FD2	FD9	FD10	FD21	FD23	FD83b	FD89	FD15	FD20	FD25	FD28	FD49F	FD86B	FD86d2	FD91c	FD92c	FD94a	FD94c
SiO_2	61.2	57.6	62.83	69.14	59.3	62.19	63.38	62.66	56.45	60.89	56.2	70.27	60.36	61.99	62.22	65.45	61.01	61	59.81
Al_2O_3	19.62	20.8	17.8	16.01	18.5	16.67	17.74	17.99	16.62	17.66	22.88	15.44	19.32	18.05	18.09	17.51	17.25	18.94	17.95
Fe_2O_3t	6.68	7.46	7.17	5.67	6.93	6.44	6.38	6.97	9.59	6.57	7.01	4.42	8.61	6.71	6.82	6.22	7.6	6.66	7.4
MnO	0.059	0.052	0.07	0.04	0.065	0.067	0.053	0.075	0.17	0.053	0.03	0.033	0.089	0.078	0.076	0.082	0.095	0.076	0.076
MgO	1.91	2.15	2.08	1.24	2.18	2.34	1.61	2.63	2.94	2.63	1.1	0.82	2.34	2.12	2.24	2.11	2.9	2.49	2.98
CaO	0.17	0.15	0.17	0.24	0.46	1.04	0.08	0.62	3.42	0.16	0.12	0.04	0.44	0.68	0.89	0.48	0.95	0.68	0.56
Na_2O	0.74	0.4	0.39	0.58	1.39	1.89	0.32	1.89	2.8	0.07	0.1	0.15	0.8	1.64	2.1	1.31	2.16	2.66	1.05
K_2O	4.32	4.88	5.64	3.44	4.57	3.98	4.9	3.92	3.36	5.75	6.1	4.2	3.82	4.39	3.9	4.11	3.82	4.33	4.7
TiO_2	0.946	0.927	0.856	0.921	0.926	0.893	0.862	0.942	2.123	0.876	1.334	1.233	0.91	0.84	0.858	0.729	0.946	0.776	0.846
P_2O_5	0.11	0.1	0.1	0.07	0.07	0.13	0.12	0.13	1.1	0.1	0.11	0.06	0.2	0.17	0.13	0.15	0.11	0.16	0.12
LOI	4.45	5.28	3.18	2.76	4.15	3.61	3.45	2.57	1.59	4.19	5.54	2.84	2.27	2.7	2.89	2.73	2.01	3.03	3.44
Total	100.2	100.1	100.5	100.1	98.55	99.25	98.88	100.4	100.2	98.96	100.5	99.5	99.16	99.37	100.2	100.9	98.85	100.8	98.95
Sc	18	20	17	14	16	16	16	18	14	18	19	13	20	15	16	15	17	15	17
Be	4	4	4	3	5	4	11	4	4	5	6	3	2	4	5	4	5	6	5
V	129	133	108	92	105	102	95	111	145	111	156	104	123	95	96	97	114	98	108
Cr	100	100	100	90	90	100	100	100	20	110	130	110	100	90	80	100	120	90	110
Co	16	17	16	13	14	12	13	16	14	14	13	9	21	18	13	15	18	15	21
Ni	50	40	40	40	40	40	40	30	< 20	40	40	30	50	30	20	40	40	40	50
Cu	30	30	90	20	10	30	50	10	50	20	50	< 10	30	20	20	20	20	40	30
Zn	100	150	80	90	100	100	80	100	110	210	80	60	130	170	90	100	110	90	150
Ga	28	30	28	24	26	25	27	25	26	28	33	24	29	28	28	24	26	23	24
Ge	2.5	2.4	2	1.7	2.3	2	3	3	2.1	2.2	1.5	1.3	3	3	2	2.4	2.8	1.7	2
As	28	137	< 5	18	20	22	6	< 5	< 5	32	10	13	< 5	13	8	0	0	8	25
Rb	164	196	223	123	221	186	231	171	220	300	372	155	186	359	263	200	257	231	262
Sr	79	49	54	92	114	196	135	159	191	20	42	88	102	112	149	102	142	134	84
Y	33.4	35.2	28	33.3	33.9	30.7	26	30	43.5	26	44.5	52.7	35	32	33	30.1	33.2	26.4	30.9
Zr	240	184	138	325	201	197	211	163	389	138	272	889	141	157	168	151	194	121	126
Nb	17.1	16.8	14.3	14.5	16.3	16.6	16	15	49.8	15.9	21.1	16.9	16	16	18	15.5	18.5	15.3	16.2
Mo	< 2	< 2	< 2	< 2	< 2	< 2	< 2	< 2	< 2	< 2	< 2	< 2	< 2	< 2	< 2	0	0	0	0
Ag	0.9	0.7	0.6	1.1	0.6	0.6	0.5	< 0.5	1.2	0.5	0.8	2.9	< 0.5	< 0.5	< 0.5	0.7	0.9	0	0.5
In	< 0.1	< 0.1	< 0.1	< 0.1	< 0.1	< 0.1	< 0.1	0.1	< 0.1	< 0.1	< 0.1	< 0.1	0.1	0.2	0.1	0.1	0.2	0.1	0.1
Sn	8	6	4	4	8	4	80	3	5	4	5	2	5	9	6	5	7	7	4
Sb	0.7	2.8	0.4	< 0.2	0.2	< 0.2	< 0.2	0.3	< 0.2	0.4	< 0.2	0.5	< 0.2	0.3	0.3	0.8	0.7	0.7	0.7
Cs	10.4	11.9	8.9	5.2	15.6	4.9	52.8	11.1	16.2	15.9	20.4	6	13.2	19.5	13.8	10.9	17.2	9.1	13.1
Ba	1011	910	958	768	735	836	618	751	272	617	662	691	981	466	431	621	406	468	552
Hf	6	4.8	3.5	8.1	5.3	5.2	5.9	4.3	8.1	3.7	7.1	22.3	4.1	4.3	4.3	4.4	5.7	3.5	3.8
Ta	1.59	1.49	1.35	1.5	1.55	1.45	1.48	1.22	3.87	1.39	1.62	1.39	1.26	1.76	1.9	1.84	1.62	1.49	1.48
W	16.4	17.6	5.4	2.3	5.7	6.2	5.8	1.6	2.1	5.8	5.2	3.5	2	2.3	2	3.6	3.5	3.6	3.5
Tl	0.64	0.61	0.56	0.27	0.84	0.67	0.92	0.66	0.77	1.45	1.14	0.45	0.76	1.81	1.23	1.18	1.3	1.23	1.46
Pb	19	21	13	15	277	24	13	19	17	37	16	7	26	21	22	25	16	12	22
Bi	0.1	0.3	< 0.1	< 0.1	0.4	0.3	0.2	0.2	0.3	0.2	0.2	< 0.1	0.2	0.5	0.3	0.9	0.7	1.8	0.3
Th	19.1	19.3	16.8	19	19.3	18.3	16.8	16.2	9.48	17.5	21.9	36.6	17.5	15.5	16.2	14.1	18.5	15.1	16
U	3.66	3.43	2.25	3.12	4.8	3.03	3.26	3.14	2.97	5.09	8.73	6.86	3.25	7.51	4	4.75	3.59	3.18	2.89

To be continued

Continuation

	Mesosomes		*Leucosomes*										*Leucogranites*									
	FD95d	FD95e	FD14	FD18	FD29	FD43b1	FD86d1	FD91a	FD92e	FD94b	FD95c	FD92d	FD16	FD30	FD48	FD58	FD70	FD86c	FD86e	FD91b	FD74	FD75
SiO_2	61.77	59.74	70.75	73.83	74.71	73.54	72.89	71.04	72.91	63.56	74.57	72.31	71.05	73.38	72.6	71.82	72.69	70.75	68.58	69.62	70.15	71.86
Al_2O_3	18.06	19.06	14.95	14.69	14.16	15.76	14.8	16.02	14.51	18.73	13.2	14.9	15.11	14.65	14.71	14.31	14.72	14.73	15.43	14.72	14.53	14.91
Fe_2O_3t	5.63	7.79	2.19	0.57	0.89	1.58	1.52	0.88	0.58	0.49	0.39	1.97	1.61	0.98	1.86	1.48	1.07	2.77	3.33	2.45	2.52	1.34
MnO	0.083	0.074	0.033	0.035	0.014	0.101	0.024	0.023	0.012	0.026	0.019	0.03	0.023	0.014	0.032	0.033	0.02	0.054	0.062	0.016	0.03	0.018
MgO	1.95	2.8	0.73	0.12	0.22	0.37	0.51	0.26	0.15	0.23	0.07	0.52	0.44	0.29	0.42	0.29	0.24	0.7	0.89	0.69	0.62	0.23
CaO	0.93	1.19	0.94	0.42	0.45	0.38	0.79	0.37	0.39	0.98	0.24	1	0.74	0.84	0.6	0.57	0.69	0.68	0.71	0.68	0.89	0.78
Na_2O	0.64	1.99	2.6	3.07	2.84	2.19	2.78	3.33	2.48	4.5	1.39	2.27	2.54	2.84	2.61	2.81	3.18	2.28	2.57	2.18	2.5	2.67
K_2O	5.11	3.93	6.52	5.92	5.36	2.89	4.55	5.78	6.71	8.68	8.73	5.7	6.01	5.07	5.26	5.32	5.56	5.15	5.55	6.16	5.58	5.31
TiO_2	0.795	0.945	0.323	0.034	0.129	0.128	0.187	0.097	0.039	0.04	0.045	0.384	0.269	0.137	0.28	0.228	0.111	0.548	0.685	0.499	0.465	0.152
P_2O_5	0.74	0.14	0.41	0.29	0.12	0.25	0.19	0.14	0.25	0.29	0.43	0.37	0.49	0.09	0.4	0.4	0.27	0.31	0.31	0.52	0.37	0.31
LOI	2.8	1.81	0.88	0.83	1.24	2.09	1.48	1.38	0.88	1.16	0.44	1.2	1.19	1.38	1.63	1.43	0.92	1.79	1.71	1.5	1.35	1.09
Total	98.52	99.47	100.3	99.82	100.1	99.28	99.73	99.32	98.9	98.69	99.53	100.7	99.47	99.67	100.4	98.69	99.47	99.77	99.83	99.03	98.99	98.68
Sc	14	17	5	2	2	3	4	1	2	1	0	2	2	2	3	2	2	4	5	1	3	1
Be	7	3	3	10	3	97	2	3	11	0	2	1	7	4	4	5	5	2	3	1	4	8
V	92	118	18	< 5	< 5	20	17	0	0	5	0	12	10	< 5	13	9	5	28	40	14	21	< 5
Cr	90	100	20	< 20	< 20	20	20	0	20	0	0	0	< 20	< 20	30	< 20	< 20	30	40	0	< 20	< 20
Co	14	18	4	1	1	3	3	1	1	1	1	3	2	1	4	2	1	7	7	1	4	1
Ni	30	40	< 20	< 20	< 20	< 20	< 20	0	0	0	0	0	< 20	< 20	< 20	< 20	< 20	< 20	< 20	0	< 20	< 20
Cu	20	20	< 10	< 10	< 10	< 10	< 10	0	30	0	0	0	< 10	< 10	< 10	< 10	< 10	< 10	< 10	0	< 10	< 10
Zn	160	110	50	< 30	< 30	40	< 30	0	0	0	0	50	60	< 30	60	80	40	90	60	80	100	70
Ga	30	27	17	16	12	24	15	12	12	10	10	20	23	13	29	24	19	25	27	26	27	22
Ge	3	2.6	1.7	3.5	1.5	5	2	1.9	3.4	2	4.1	1.2	1.2	1.8	2	2	2	2	2	1.5	2	2
As	0	0	< 5	< 5	< 5	< 5	< 5	0	7	0	0	0	< 5	< 5	< 5	5	< 5	24	13	9	7	< 5
Rb	359	191	192	239	150	291	162	174	191	231	339	141	206	142	324	379	314	222	270	346	393	358
Sr	190	226	181	48	264	77	208	187	106	170	102	215	102	227	63	78	88	127	149	69	74	89
Y	31.8	33.3	17.8	6.2	9.9	5	18	12.8	5.1	11.2	2.9	7.8	9.1	17.4	10	9	9	18	17	13.2	15	5
Zr	232	173	141	15	56	34	50	9	14	12	23	125	107	46	114	86	41	227	284	215	219	50
Nb	45.1	18.9	5.3	5.1	2.9	16	3	4.3	2.1	1.7	5.8	6.5	10.4	3.5	6	4	6	6	7	4.8	5	11
Mo	0	0	< 2	< 2	< 2	< 2	< 2	0	0	0	3	0	< 2	< 2	< 2	< 2	< 2	< 2	12	0	< 2	< 2
Ag	0.8	0.8	0.5	< 0.5	< 0.5	< 0.5	< 0.5	0	0	0	0	0.6	< 0.5	2.1	< 0.5	< 0.5	< 0.5	0.5	0.6	1	0.5	< 0.5
In	0.4	0.1	< 0.1	< 0.1	< 0.1	0.1	< 0.1	0	0	0	0	0	< 0.1	< 0.1	0.1	0.1	< 0.1	< 0.1	< 0.1	0.1	0.1	0.1
Sn	67	4	5	18	3	43	3	4	8	6	15	3	8	5	8	10	7	5	3	3	5	12
Sb	0.7	0.6	< 0.2	< 0.2	< 0.2	< 0.2	< 0.2	0.7	0.6	0.6	0.7	0.7	< 0.2	< 0.2	< 0.2	< 0.2	< 0.2	< 0.2	< 0.2	1	< 0.2	< 0.2
Cs	22.8	9.5	5.6	22.9	5.3	16.3	4.1	2.9	9.9	4	17.3	3.5	9.1	7.1	5.9	22.5	11	4.7	5.9	4.2	5.1	25.7
Ba	919	773	910	107	530	201	716	523	443	851	129	552	494	425	295	295	281	508	596	290	365	175
Hf	6.6	5	3.9	0.6	1.8	1.4	1.3	0.4	0.6	0.5	1.2	3.8	3	1.5	2.6	2.4	1.2	6	7.8	6.3	5.8	1.7
Ta	12	1.49	0.78	2.05	0.47	18.5	0.69	1.04	0.83	0.7	4.49	0.57	1.98	0.64	0.99	0.84	1.14	0.58	0.52	0.42	0.56	1.93
W	4.3	3.6	2.8	3.8	2.7	4.2	< 0.5	3.4	3.2	2.6	2.4	2.3	3.3	5.2	2.3	1.3	0.5	2.6	3.5	3.5	1.3	1.6
Tl	1.66	0.93	0.64	0.78	0.45	1	0.82	0.93	0.89	1.48	1.76	0.64	0.77	0.38	1.82	2.02	1.49	1.19	1.45	1.83	2.03	1.83
Pb	18	21	47	47	48	17	31	50	59	45	27	63	39	55	29	42	43	35	29	31	34	40
Bi	0.4	0.4	0.1	0.5	0.2	0.4	0.3	1.1	1.5	0.5	0.1	0	0.8	0.6	0.4	0.4	0.8	0.2	0.1	0.1	0.2	0.9
Th	16.8	18.8	19.4	0.95	5.04	2.54	5.49	2.1	0.69	1.65	0.85	21.3	9.08	7	15.4	14.4	3.36	59.2	64.1	46.7	53.4	4.42
U	7.46	3.02	7.37	1.79	3.05	6.92	1.97	1.1	1.71	18.2	2.92	6.57	7.56	3.8	5.7	5.33	3.74	4.76	8.03	4.79	13.4	2.88

To be continued

Continuation

	Douro Group								***Mesosomes***												
	FD1	FD2	FD9	FD10	FD21	FD23	FD83b	*FD89*	FD15	FD20	FD25	FD28	FD49F	FD86B	FD86d2	FD91c	FD92c	FD94a	FD94c	FD95d	FD95e
La	58.1	61	50.7	55.1	61.3	52.5	56.9	53.3	59.1	50.3	71.6	75.7	54.5	52.1	49.6	43.6	55.6	46.4	50.9	46.4	58.6
Ce	115	119	97.5	112	114	105	109	98.9	123	96.4	144	160	107	104	94.4	84.8	109	88.2	96.5	90.9	112
Pr	13.3	13.7	11.3	12.8	13.8	11.8	12.3	11.9	15	11.1	16.4	18	12.1	11.3	10.8	9.73	12.1	10	10.9	10.6	12.6
Nd	46.5	48.5	39.1	46.5	49.5	41.5	44.3	42.7	59.9	39	59.4	65.5	45.3	41.8	40	36.9	45.9	37.3	40.1	40.5	47.7
Sm	8.86	9.07	7.2	8.97	9.09	8.01	8.17	8.11	13	7.23	11.5	12.4	8.71	7.71	7.56	7.23	8.85	6.99	7.78	7.84	9.15
Eu	1.81	1.84	1.15	1.59	2.02	1.52	1.68	1.61	2.98	1.18	1.66	1.66	1.83	1.27	1.28	1.56	1.35	1.44	1.43	1.73	1.65
Gd	7.05	7.53	5.98	6.85	7.36	6.56	5.96	6.34	11.3	5.82	9.08	10.3	7.13	6.22	6.41	6.23	7.16	5.8	6.59	6.62	7.48
Tb	1.11	1.1	0.88	1.06	1.08	0.96	0.91	0.96	1.65	0.86	1.41	1.62	1.14	0.98	0.95	0.92	1.03	0.86	0.98	1.01	1.06
Dy	6.28	6.43	5.11	6.06	6.33	5.64	5	5.76	9.15	4.91	8.1	9.26	6.67	5.62	5.75	5.42	6.07	4.87	5.63	5.86	6.04
Ho	1.18	1.23	0.99	1.17	1.18	1.11	0.93	1.07	1.62	0.94	1.52	1.76	1.27	1.09	1.12	1.06	1.17	0.91	1.11	1.11	1.13
Er	3.43	3.52	2.8	3.44	3.33	3.11	2.87	3.2	4.22	2.64	4.32	5.28	3.73	3.08	3.4	3.06	3.31	2.7	3.15	3.25	3.32
Tm	0.497	0.497	0.413	0.5	0.464	0.457	0.407	0.457	0.599	0.371	0.613	0.793	0.532	0.45	0.475	0.458	0.485	0.387	0.449	0.505	0.468
Yb	3.28	3.3	2.72	3.21	3.06	2.94	2.61	3.04	3.6	2.4	4.09	5.15	3.57	3.09	3.13	2.94	3.1	2.37	2.92	3.54	3.08
Lu	0.515	0.524	0.414	0.488	0.461	0.445	0.408	0.473	0.508	0.372	0.631	0.798	0.556	0.456	0.467	0.475	0.476	0.352	0.448	0.564	0.454
∑REE	266.9	277.2	226.2	259.7	272.9	241.5	251.4	237.8	305.6	223.5	334.32	368.2	254	239.1	225.3	204.4	255.6	208.9	228.9	220.4	264.7
Eu/Eu*	0.68	0.66	0.52	0.59	0.73	0.62	0.70	0.66	0.74	0.54	0.48	0.44	0.69	0.54	0.55	0.69	0.50	0.67	0.60	0.72	0.59
La_N/Yb_N	11.96	12.48	12.58	11.59	13.52	12.05	14.71	11.83	11.08	14.15	11.82	9.92	10.30	11.38	10.70	10.00	12.11	13.21	11.77	8.85	12.84

Table 2: Rare earth elements (ppm) of Douro Group, mesosomes, leucosomes and leucogranites.

Tabela 2: Composição química em terras raras das amostras do Grupo do Douro, mesossomas, leucossomas e leucogranitos.

	Douro Group								***Mesosomes***											
	FD1	FD2	FD9	FD10	FD21	FD23	FD83b	*FD89*	FD15	FD20	FD25	FD28	FD49F	FD86B	FD86d2	FD91c	FD92c	FD94a	FD94c	FD95d	FD95e
La	58.1	61	50.7	55.1	61.3	52.5	56.9	53.3	59.1	50.3	71.6	75.7	54.5	52.1	49.6	43.6	55.6	46.4	50.9	46.4	58.6
Ce	115	119	97.5	112	114	105	109	98.9	123	96.4	144	160	107	104	94.4	84.8	109	88.2	96.5	90.9	112
Pr	13.3	13.7	11.3	12.8	13.8	11.8	12.3	11.9	15	11.1	16.4	18	12.1	11.3	10.8	9.73	12.1	10	10.9	10.6	12.6
Nd	46.5	48.5	39.1	46.5	49.5	41.5	44.3	42.7	59.9	39	59.4	65.5	45.3	41.8	40	36.9	45.9	37.3	40.1	40.5	47.7
Sm	8.86	9.07	7.2	8.97	9.09	8.01	8.17	8.11	13	7.23	11.5	12.4	8.71	7.71	7.56	7.23	8.85	6.99	7.78	7.84	9.15
Eu	1.81	1.84	1.15	1.59	2.02	1.52	1.68	1.61	2.98	1.18	1.66	1.66	1.83	1.27	1.28	1.56	1.35	1.44	1.43	1.73	1.65
Gd	7.05	7.53	5.98	6.85	7.36	6.56	5.96	6.34	11.3	5.82	9.08	10.3	7.13	6.22	6.41	6.23	7.16	5.8	6.59	6.62	7.48
Tb	1.11	1.1	0.88	1.06	1.08	0.96	0.91	0.96	1.65	0.86	1.41	1.62	1.14	0.98	0.95	0.92	1.03	0.86	0.98	1.01	1.06
Dy	6.28	6.43	5.11	6.06	6.33	5.64	5	5.76	9.15	4.91	8.1	9.26	6.67	5.62	5.75	5.42	6.07	4.87	5.63	5.86	6.04
Ho	1.18	1.23	0.99	1.17	1.18	1.11	0.93	1.07	1.62	0.94	1.52	1.76	1.27	1.09	1.12	1.06	1.17	0.91	1.11	1.11	1.13
Er	3.43	3.52	2.8	3.44	3.33	3.11	2.87	3.2	4.22	2.64	4.32	5.28	3.73	3.08	3.4	3.06	3.31	2.7	3.15	3.25	3.32
Tm	0.497	0.497	0.413	0.5	0.464	0.457	0.407	0.457	0.599	0.371	0.613	0.793	0.532	0.45	0.475	0.458	0.485	0.387	0.449	0.505	0.468
Yb	3.28	3.3	2.72	3.21	3.06	2.94	2.61	3.04	3.6	2.4	4.09	5.15	3.57	3.09	3.13	2.94	3.1	2.37	2.92	3.54	3.08
Lu	0.515	0.524	0.414	0.488	0.461	0.445	0.408	0.473	0.508	0.372	0.631	0.798	0.556	0.456	0.467	0.475	0.476	0.352	0.448	0.564	0.454
∑REE	266.9	277.2	226.2	259.7	272.9	241.5	251.4	237.8	305.6	223.5	334.32	368.2	254	239.1	225.3	204.4	255.6	208.9	228.9	220.4	264.7
Eu/Eu*	0.68	0.66	0.52	0.59	0.73	0.62	0.70	0.66	0.74	0.54	0.48	0.44	0.69	0.54	0.55	0.69	0.50	0.67	0.60	0.72	0.59
La_N/Yb_N	11.96	12.48	12.58	11.59	13.52	12.05	14.71	11.83	11.08	14.15	11.82	9.92	10.30	11.38	10.70	10.00	12.11	13.21	11.77	8.85	12.84

	Leucosomes										***Leucogranites***									
	FD14	FD18	FD29	FD43b1	FD86d1	FD91a	FD92e	FD94b	FD95c	FD92d	FD16	FD30	FD48	FD58	FD70	FD86c	FD86e	FD91b	FD74	FD75
La	38.9	3.36	12	7.37	16.2	6.4	2.24	8.38	6	51.9	25.8	16.3	22.8	21.8	9.03	55.6	55.4	33.9	64.1	13.1
Ce	82.8	5.8	25.2	13.3	31.3	11.9	3.75	15.2	7.62	111	53.7	34.3	53.5	49.8	19.5	137	163	112	155	27.3
Pr	9.83	0.63	2.88	1.52	3.47	1.34	0.45	1.77	0.88	13	6.38	3.83	6.44	6.08	2.26	16.7	16.3	11.4	18.9	3.13
Nd	36.2	2.18	9.86	5.18	12.6	4.74	1.9	6.67	3.01	48.6	22.3	13.1	22.1	23	8.66	63.4	60.8	45	70.4	11.8
Sm	7.97	0.66	2.29	1.2	2.76	1.18	0.49	1.54	0.54	11.2	5.11	3.24	5.09	5.15	2.49	12.2	12.1	11.7	13.5	3.31
Eu	1.36	0.268	1.49	0.424	1.28	0.899	0.68	1.01	0.259	1.87	0.647	1.07	0.529	0.58	0.597	0.926	0.868	0.497	0.706	0.755
Gd	6.18	0.66	2.17	0.84	2.65	1.28	0.45	1.7	0.41	6.82	4.6	2.91	3.37	3.85	2.33	6.6	6.93	7.53	7.07	2.95
Tb	0.82	0.13	0.35	0.17	0.42	0.29	0.11	0.29	0.07	0.61	0.65	0.5	0.59	0.5	0.38	0.83	0.8	0.93	0.76	0.34
Dy	3.83	0.94	1.87	0.97	2.84	1.97	0.76	1.81	0.44	1.83	2.72	3.08	2.67	2.14	2.09	3.76	3.54	3.42	3.35	1.25
Ho	0.62	0.19	0.33	0.17	0.6	0.38	0.17	0.34	0.08	0.27	0.33	0.55	0.32	0.29	0.27	0.61	0.56	0.44	0.49	0.16
Er	1.61	0.59	0.86	0.51	1.7	1.04	0.56	1.06	0.27	0.69	0.68	1.59	0.76	0.78	0.67	1.64	1.47	0.94	1.24	0.43
Tm	0.222	0.11	0.127	0.082	0.251	0.173	0.11	0.161	0.051	0.086	0.076	0.25	0.114	0.115	0.095	0.226	0.183	0.115	0.167	0.06
Yb	1.43	0.88	0.83	0.6	1.83	1.11	0.68	1.09	0.38	0.49	0.44	1.58	0.65	0.67	0.52	1.35	1.07	0.63	0.98	0.37
Lu	0.209	0.147	0.131	0.092	0.262	0.168	0.108	0.168	0.06	0.07	0.065	0.23	0.098	0.087	0.071	0.205	0.164	0.074	0.136	0.05
∑REE	191.9	16.5	60.4	32.4	78.1	32.9	12.5	41.2	20.1	248.4	123.5	82.5	119	114.8	48.9	301	323.1	228.6	336.8	65
Eu/Eu*	0.57	1.23	2.01	1.23	1.43	2.23	4.35	1.90	1.62	0.61	0.40	1.04	0.37	0.38	0.75	0.29	0.27	0.15	0.20	0.72
La_N/Yb_N	18.36	2.58	9.76	8.29	5.98	3.89	2.22	5.19	10.66	71.49	39.58	6.96	23.68	21.96	11.72	27.80	34.95	36.32	44.15	23.90

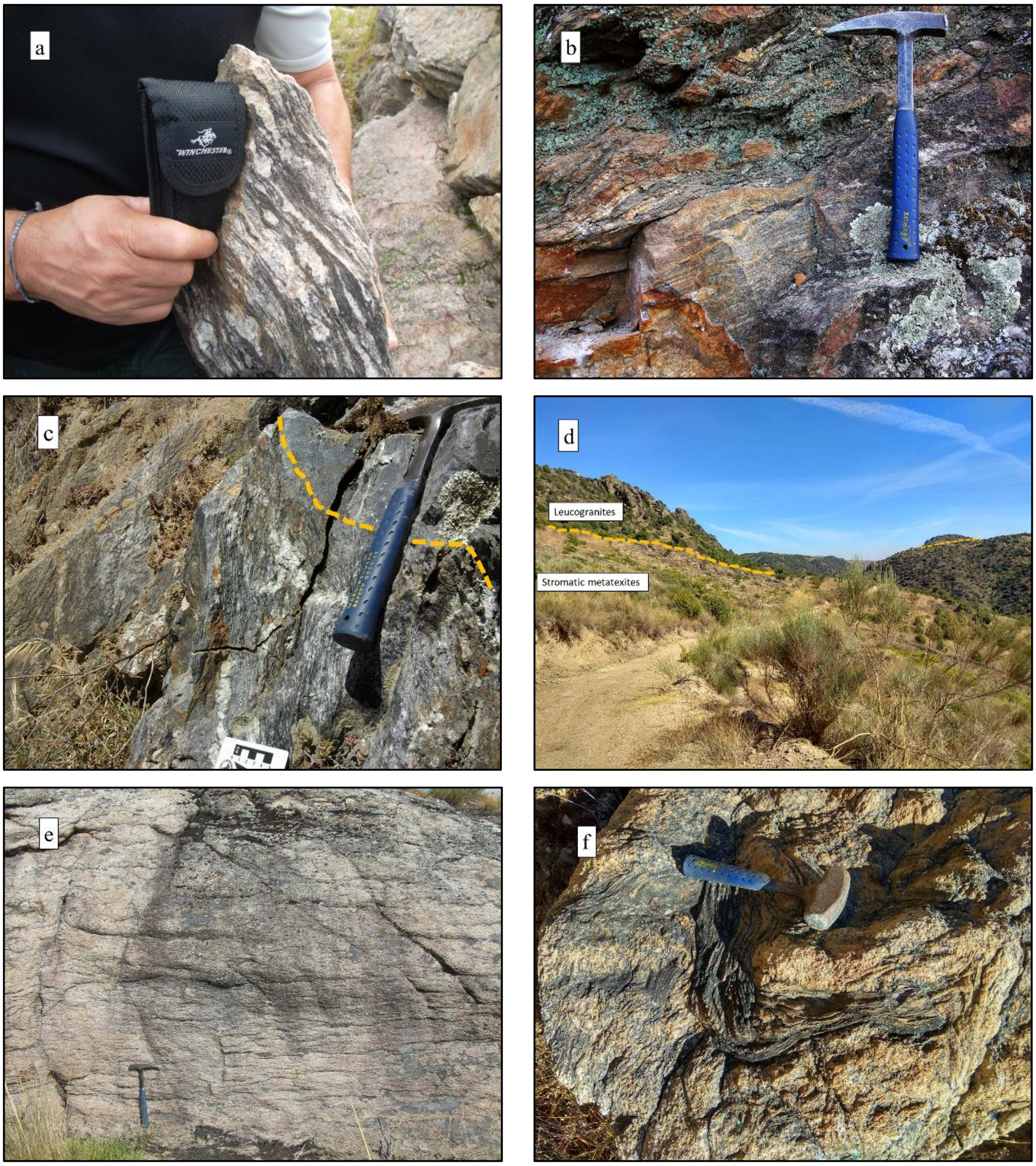

Figure 2. (a) Detail of the stromatic metatexites showing the alternation between quartz-feldspathic bands (leucosomes) and dark biotite-sillimanite-rich layers (mesosomes); (b) field aspect of the metatexites showing the stromatic structure concordantly to S_2 foliation; (c) metapsamitic rock enclosed by the stromatic metatexite; (d) geomorphologic aspect of the leucogranite sill above the stromatic metatexites. Note that the sub-horizontal contact between them, is marked with dashes; (e) mesoscopic aspect of the leucogranite sill; (f) leucogranite displaying a metasedimentary enclave.

Figura 2. (a) Detalhe dos metatexitos estromáticos mostrando a alternância entre bandas quartzo-feldspáticas (leucossomas) e faixas escuras ricas em biotite e sillimanite (mesossomas); (b) Aspeto dos metatexitos estromáticos concordantes com a foliação S_2; (c) metatexito estromático mostrando um nódulo resistente de rocha metapsamítica; (d) aspeto geomorfológico do leucogranito contactanto com os metatexitos estromáticos. Note-se a linha tracejada a marcar o limite sub-horizontal entre os dois; (e) aspeto mesoscópico do leucogranito; (f) enclave metassedimentar no leucogranito.

Biotite constitutes aligned sub-idiomorphic crystals that often include accessory minerals such as, zircon, monazite and rutile (Fig. 4b). The biotite crystals have XMg = (Mg/Mg + Fe) ratios ranging from 0.32 to 0.46. Titanium content is relatively high, varying between 0.29 and 0.43 atoms per formula unit (a.p.f.u) and Mn content is low (0.02 to 0.05 a.p.f.u). Biotites from mesosomes are plotted in the annite-siderophilite series field. Sillimanite is aligned with biotite and occur mainly as fibrous. Despite that, sillimanite also appear in some mesosomes as prismatic crystals with diamond shape. Analysed plagioclase from mesosomes range between oligoclase-andesine (An25-39) and K content is very low (<0.01 a.p.f.u).

The abundance of biotite together with sillimanite and the absence of primary muscovite and garnet in the mesosomes, show that the partial melting conditions was controlled by muscovite-dehydration reactions, producing melt, and sillimanite and K-feldspar as peritectic minerals. This reaction is interpreted as the metamorphic peak, which should have been attained during D_2.

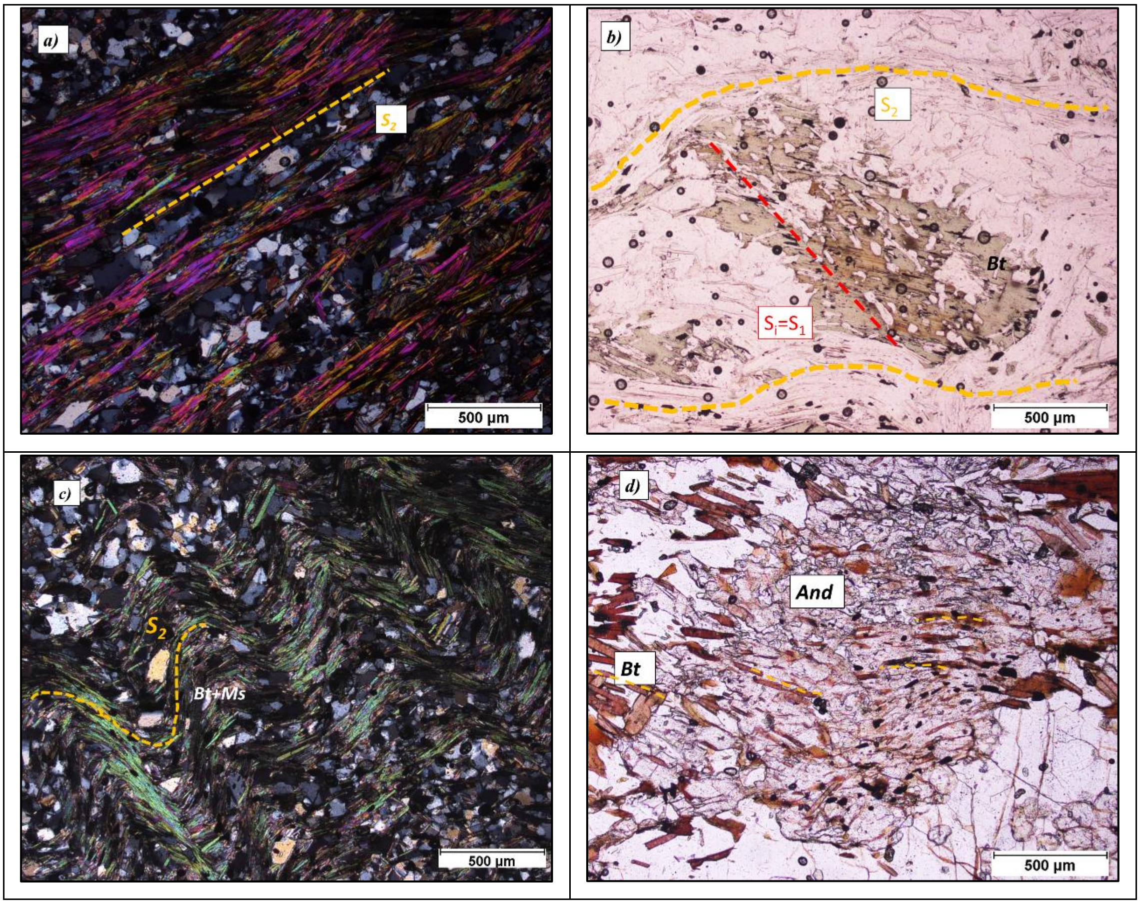

Figure 3. Photomicrographs of Douro group metasediments. (a) S_2 foliation marked by biotite and muscovite alignment in metasedimentary sample; (b) Pre-S_2 poikiloblast of biotite showing inclusion trails, evidencing a previous foliation ($S_i = S_1$); (c) S_2 foliation folded by D_3 in metasedimentary sample; (d) Post-S_2 poikiloblast of andalusite showing inclusions of biotite that grew during the development of S_2 foliation.

Figura 3. Micrografias dos metassedimentos do Grupo do Douro. (a) foliação S_2 marcada pelo alinhamento das micas; (b) poeciloblasto de biotite Pré-S_2 com inclusões alinhadas, evidenciando uma foliação prévia ($S_i = S_1$); (d) metassedimento marcado por uma foliação S_2 afetada por dobras D_3; (d) poeciloblasto de andalusite Pós-S_2 mostrando inclusões orientadas de biotite.

Leucosomes have igneous textures (Fig. 4c), are coarser than mesosomes and some of them have solid deformation evidence with variable extent and intensity. The igneous fabric has heterogranular texture and medium- to coarse-grained size, acquiring sometimes pegmatitic textures. They are composed dominantly by quartz (30-35%), K-feldspar (25-30%) and plagioclase (15-20%) with minor contents of biotite, muscovite, garnet, sillimanite, tourmaline, apatite and zircon. Quartz forms xenomorphic crystals with variable dimensions (0.1-2 mm), showing straight or jagged contacts with other crystals. The deformation evidences include sub-granulation, undulating extinction, dynamic recrystallization and sutured boundaries. The potassic feldspar corresponds to microcline and forms xenomorphic to subidiomorphic crystals. The microcline crystals show pericline twinning and may contain micropertitic textures. They may also exhibit straight or sutured crystalline shapes and may have recrystallized boundaries, indicating deformation under subsolidus conditions at high temperatures. Microcline contains variable amounts of Na (0.05 - 0.31 a.p.f.u) and Ba content is low (< 0.02 a.p.f.u).

Plagioclase is frequently twinned on the albite law, shows compositional zoning and their composition ranges from andesine to albite (An30-An6). Their crystals sometimes show deformation signs like flame-shape twinning, dislocation of twinning and sutured boundaries. Biotite, sillimanite and other minor phases, except garnet, occur in remains of aligned mesosomes in leucosomatic matrix or otherwise, as dispersed isolated crystals within the matrix. The biotite of the leucosomes have similar compositions to the mesosomes with XMg = (Mg/Mg + Fe) ratios ranging from 0.27 to 0.41, relatively high Ti content (0.32 - 0.47 a.p.f.u) and low Mn (0.02 - 0.04 a.p.f.u).

Garnet is corroded and may contain inclusions of globular quartz, being interpreted to as a peritectic phase (Fig. 4d). Their presence in these rocks seems to suggest that melts resulted from anatexis of metasedimentary rocks through biotite dehydration reactions, at slightly deeper structural levels. According to the evidence, the anatectic melts were produced in depth and were injected into their host during D_2, letting a garnet-richest residum in depth. The absence of melanosomes in the leucosomes margins empathizes the idea that they are not in situ and have been injected in the BMC like leucosome veins (Sawyer, 2008; Morfin *et al.*, 2013). Therefore, it is considered that CMB shows petrographic evidences that it is a Migmatitic Injection Complex generated during the extensional deformation D_2 (Leitch and Weinberg, 2012; Morfin *et al.*, 2013, 2014).

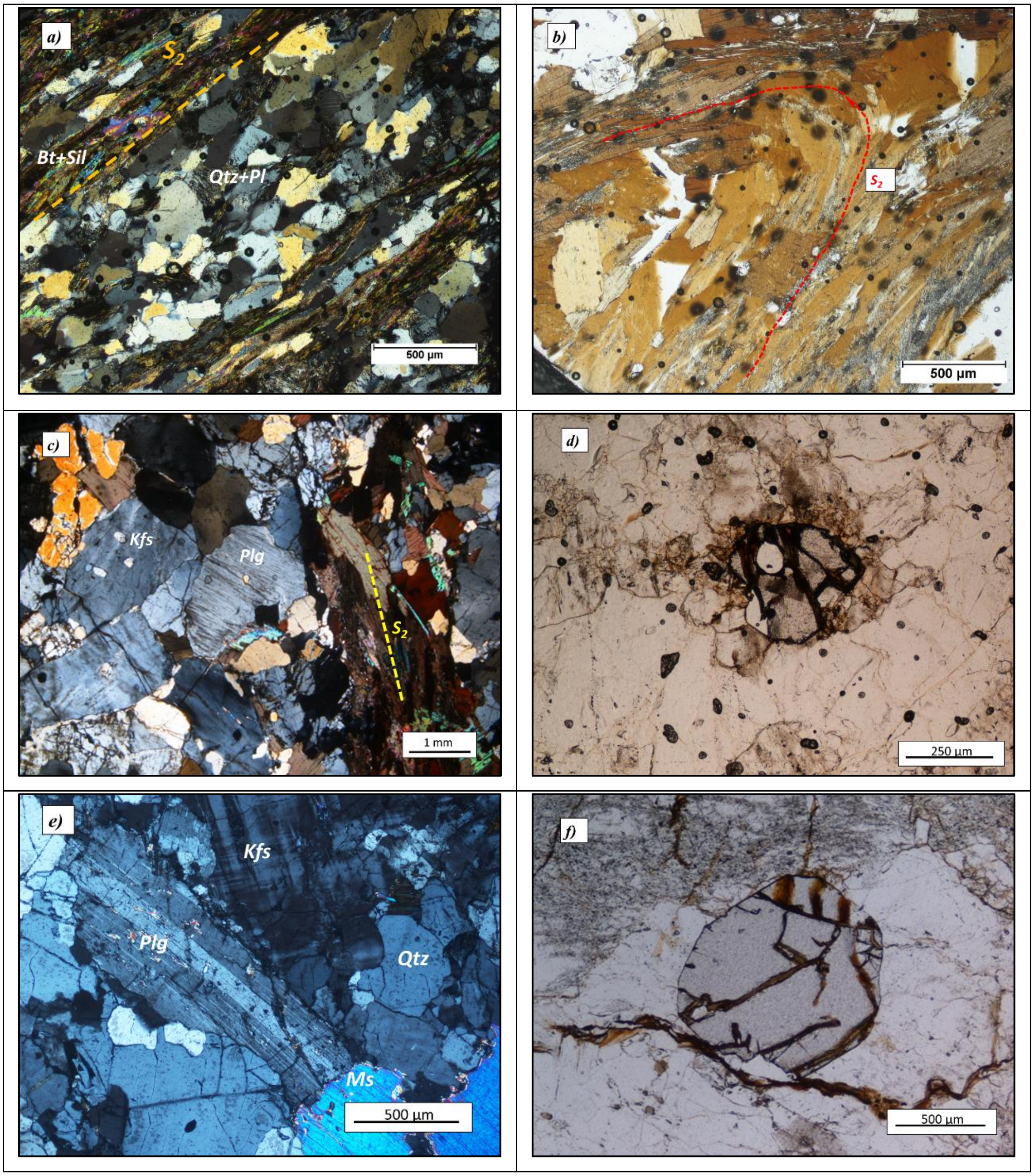

Figure 4. Photomicrographs of CMB rocks. (a) mesosome sample showing the alternance of biotite-sillimanite-rich and highly recrystallized quartz-feldspar layers; (b) detail of the biotite and sillimanite defining a polygonal arc on S_2 foliation in mesosome. Note that the abundance of pleochroic halos around zircon included in the biotite; (c) leucosome composed by K-feldspar and plagioclase with no evidence of solid-deformation; (d) peritectic garnet with quartz inclusion in the leucosome matrix; (e) medium-grained leucogranite showing quartz, microcline, plagioclase and muscovite; (f) idiomorphic garnet in the leucogranite sample.

Figura 4. Microfotografias das rochas migmatíticas do CMB. (a) amostra de mesosoma mostrando a alternância entre as faixas ricas em biotite e sillimanite e bandas quartzo-feldspáticas recristalizadas; (b) mesosoma exibindo a biotite e silimanite um arco poligonal sobre a microcharneira S_2, atestando o carater pós-cinemático. Observa-se uma grande abundância em zircões incluídos na biotite; (c) leucossoma composto por feldspato potássico e plagioclase que não mostram evidências de deformação no estado sólido; (d) leucossoma composto por granada peritética mostrando inclusões de quartzo; (e) leucogranito de grão médio composto por quartzo, microcline, plagioclase e muscovite; (f) granada idiomófica em amostra de leucogranito.

Chemical data of garnet reveal that their composition is dominated by end-members almandine (XAlm = 0.49 - 0.79) and spessartine (XSps = 0.13 - 0.5) and low contents in pyrope (Xpy= 0.04 - 0.07) and grossular (XGrs= 0.01 - 0.03). Their zoning is generally homogeneous, despite of subtle decreases of XAlm, Xpy and XGrs and small increase of XSps on the edge of the garnets. These chemical changes are attributed to retrograde garnet consumption by net transfer reactions (Brown, 2002).

The evidences of deformation observed in leucosomes are heterogeneous. However, it is notorious that folded leucosomes are not always affected by deformation, preserving igneous fabric. The deformation seems to have been more intense in leucosomes of stromatic metatexites that was affected by D_3-

shear zones. Based on this feature, the leucosomes should have crystallized during the D_3, when shear deformation acted.

The leucogranites are mainly composed by quartz, microcline, plagioclase, biotite, muscovite (Fig. 4e). The identified accessory minerals are tourmaline, sillimanite, garnet, apatite, monazite and zircon. The microcline (30 - 35%) is more abundant then plagioclase (20 - 25%). The microcline in leucogranites has less Na content than leucosomes (0.02 - 0.10 a.p.f.u) and Ba content also is low. Plagioclase is twinned on the albite law and their composition is more uniform (An2-An10). The proportion between biotite and muscovite is variable and together they often define an orientation concordant with D_2 structures, typical of diatexites. Biotite have XMg = (Mg/Mg+Fe) ratios tend to be lower between 0.25 and 0.33 a.p.f.u, low Ti content (0.01 - 0.1 a.p.f.u) and low Mn (0.02 - 0.05 a.p.f.u). The observed garnet has the same characteristics to those of leucosomes (Fig. 4f).

Such as in the leucosomes, the leucogranites have igneous fabric but not always show evidences of deformation, leading to support that crystallization of the melts still occurred during the D_3, but should have been more intense near to strike-slip sub-vertical shear zones.

6. Whole-Rock Geochemistry

The Douro Group metasediments show solid evidences that they are the likely protolith of stromatic metatexites and leucogranites that occur in the BMC. For this reason, it is relevant to compare metasediments together with BMC rocks using Harker variation diagrams (Fig. 5).

The variation diagrams reveal significative differences between Douro Group metasediments, mesossomes and leucosomes from stromatic metatexites and associated leucogranites. The Douro Group metasedimentary rocks and mesosomes have remarkable similarities with lower content in SiO_2, Na_2O, K_2O, CaO and P_2O_5 and higher content in Fe_2O_3, MgO, TiO_2, MnO and Al_2O_3, defining the most mafic segment of the sequence. The composition of metasedimentary rocks reflects specially the abundance of phyllosilicates and, in the case of mesosomes, the greater abundance of biotite and sillimanite. The remarkable chemical similarity presented by metasediments and mesosomes suggest that Douro Group represented an important source of fertile material involved in variscan anatexis event.

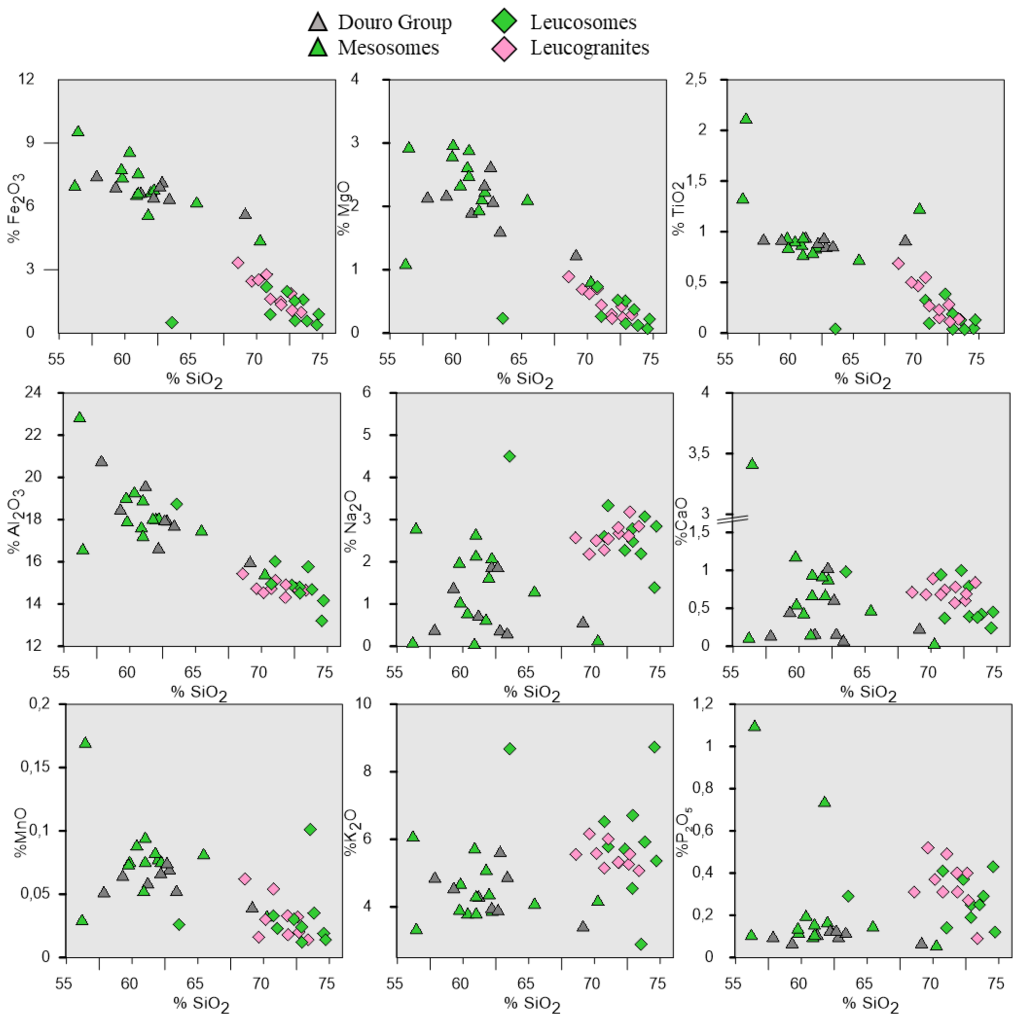

Figure 5. Harker diagrams of major element of Douro Group metasediments, mesosomes, leucosomes and leucogranites.

Figura 5. Diagramas de Harker para os elementos maiores dos metassedimentos do Grupo do Douro, mesossomas, leucossomas e leucogranitos.

Leucosomes and leucogranites are plotted in the acid extreme of the diagrams (SiO_2 > 63.56%), describing coherent alignments with mesosomes and metasedimentary rocks. They reveal lower contents in Fe_2O_3, MgO, TiO_2, MnO, CaO, Al_2O_3 and higher contents in Na_2O, K_2O and P_2O_5 compared to mesosomes and Douro Group. The increment of SiO_2 together with Na_2O and K_2O observed in these samples is compatible with rocks that resulted from crystallization of the anatectic melts with modal compositions dominated by quartz and feldspars. Some leucogranites have higher contents of Fe_2O_3, TiO_2, MnO and P_2O_5, indicating that melts may have retained residual crystals in their composition (i.e. biotite, apatite or garnet) (Bea *et al*., 1994; Bea 1996; Milord *et al*., 2001; Solar *and* Brown, 2001).

CIPW norm for studied igneous samples was calculated and Ab, An and Or molecules were plotted in ternary diagram, proposed by O'Connor (1965) and modified by Barker (1979) (Fig. 6). Leucosomes and leucogranites are projected at the bottom of the diagram and fall within granite field. Leucosomes are scattered along the granite field but all of them reveal Or molecule enrichment suggesting that may have occurred accumulation of K-feldspar during magmatic evolution of the melts. On the other hand, the leucogranites show less variability (constant Ab/Or) and should not represent compositions affected by feldspar accumulation. The normative An content is not significant indicating that plagioclase composition is dominated by Ab molecule.

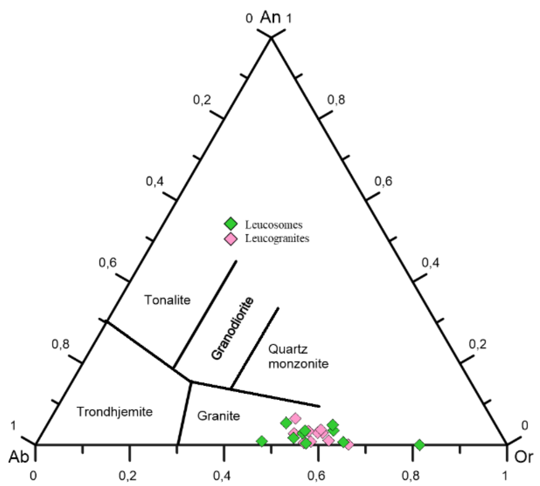

Figure 6. Normative Anorthite–Albite–Orthoclase diagram for leucosomes and leucogranites, proposed by O'Connor (1965) and modified by Barker (1979).

Figura 6. Diagrama Anortite-Albite-Ortoclase (proposto por O'Connor (1965) e modificado por Barker (1979) onde se projetam as composições normativas dos leucossomas e leucogranitos.

Multi-element diagrams for Douro Group metasediments and BMC rocks normalized to the primitive mantle (Sun *and* McDonough, 1989) are given in figure 7. Despite some variability, particularly in leucosomes and leucogranites, the analysed rocks have similar-shaped patterns with positive LILE/HFSE (Rb_N/Yb_N and Th_N/Zr_N) and negative anomalies in Ba, Nb, Sr and Ti. The similarity between them suggests once again that anatectic melts resulted from partial melting of rocks with equivalent composition of Douro Group.

Mesosomes have multi-element patterns that closely resemble those of the Douro group metasedimentary rocks with negative anomalies in Ba, Nb, Sr, P and Ti, reflecting that rocks inherited these features from source rocks. Despite some variability, leucosomes show sloping patterns with positive Rb_N/Yb_N and Th_N/Zr_N, marked negative Th, Nb and Ti anomalies and positive inflections in Rb, K, Ta e P. These features are compatible with the abundance of K-feldspar (positive anomalies in K and Rb) and the absence of biotite (anomalies in Th and Nb and marked negative anomaly in Ti). The positive anomalies in Ta and P and the variable concentration noted by the transition elements, suggest the presence of accessory minerals in some leucosomes, such as apatite, monazite and zircon.

Leucogranites also have steep patterns with negative anomalies in Nb, Sr and Ti and positive inflections in Rb and K. Their patterns are compatible with fractionated melts (steady positive K-anomaly and negative anomaly in Sr). The variable concentration observed in Th, Ti and transition elements indicate the presence of biotite and accessory minerals. This geochemical feature expresses that some leucosomes and leucogranites may have retained residual crystals in their composition (*i.e.* biotite, apatite, monazite and zircon) (Bea *et al*., 1994; Bea, 1996; Milord *et al*., 2001; Solar and Brown, 2001).

Chondrite normalized REE contents (Evensen *et al*., 1978) for Douro Group and BMC rocks are given in figure 8. REE patterns for Douro Group metasedimentary rocks exhibit a considerable enrichment in REE ($\sum$REE = 226.2 – 277.2 ppm), a moderate fractionation with LREE/HREE positive (La_N/Yb_N = 11.59 – 14.71) and negative Eu-anomalies (Eu/Eu* = 0.52 – 0.73) (Fig. 8a).

REE patterns of mesosomes (Fig. 8b) match with Douro Group REE patterns, indicating that they have similar sedimentary origin and attest the involvement of these rocks in the anatexis (mesosomes: $\sum$REE = 204.4 – 368.2 ppm; La_N/Yb_N = 8.85 – 14.15; Eu/Eu* = 0,44 – 0.74). Mesosomes tend to present an REE-enrichment compared to metasedimentary rocks from Douro Group. This observation may be attributed to the high biotite content in the mesosomes. As previously reported by the petrographic observations, biotite of mesosomes often encloses accessory REE-minerals, being responsible to elevate the REE content.

Based on the REE patterns of leucosomes, it is possible to distinguish the following two major groups: (1) positive Eu-anomaly leucosomes (Fig. 8c); (2) negative Eu-anomaly leucosomes (Fig. 8d). The first group and the most numerous, is characterized by a REE depletion ($\sum$REE = 12.5 – 78.1 ppm) and marked positive Eu-anomalies (Eu/Eu* = 1.23 – 4.35), indicating a mineral composition dominated by plagioclase and suggesting the accumulation of this mineral during the magmatic evolution of the anatectic melts (Ellis and Obata, 1992; Johannes *et al*., 2003). Based on the petrography and geochemical data, the positive Eu-anomaly is attributed to greater abundance of K-feldspar.

The leucosomes from the second group are enriched in the REE ($\sum$REE = 191.9 – 248.4 ppm) and their REE patterns are sloping with high LREE/HREE (La_N/Yb_N = 18.36 – 71.49) and negative Eu-anomalies (Eu/Eu* = 0.57 – 0.60). These characteristics suggest that leucosomes can resulted from the crystallization of the evolved melts that underwent by fractionated crystallization (Ellis and Obata, 1992; Johannes *et al*., 2003). However, the enrichment in LREE also indicates the presence of residual minerals, such as zircon or apatite (Milord *et al*., 2001; Solar and Brown, 2001).

The leucogranites exhibit relative heterogeneity in REE concentration, being possible to identify two main groups. The first group (Fig. 8e) is characterized by an enrichment of REE (∑REE = 114.8 – 336.8 ppm), REE patterns with high LREE/HREE rates (La_N/Yb_N = 21.96 – 44.15) and marked negative Eu-anomalies (Eu/Eu* = 0.15 – 0.40). Their REE patterns support that the precursor melts were produced by high partial melting rates, allowing a higher dissolution of residual mineral phases in the melt (enrichment of REE) (Ayres and Harris, 1997). The negative Eu-anomaly verified in this group indicates that leucogranites crystallized from fractionated granitic melts (no evidences of feldspar accumulation).

The second group of leucogranites (Fig. 8f) is characterized by a lower REE content ((∑REE = 48.9 – 82.5 ppm) and REE patterns with low to moderate LREE/HREE (La_N/Yb_N = 6.96 – 23.9) and small negative to positive Eu-anomalies (Eu/Eu*= 0.72 – 1.04). Their REE patterns, together with the lower TiO_2 and Zr contents, may to express that leucogranites from second group are depleted in accessory minerals. In petrography analysis it was observed that accessory minerals phases (ex: zircon, rutile, monazite) are sequestered as inclusions in biotite of the mesosomes. This suggests that precursor melts may have been generated through low melting rates of Douro Group, where it was not attained the biotite dehydration, explaining the lower contents of REE and consequently the lower abundance of accessory minerals in these granites (Watt and Harley, 1993; Bea 1996; Milord *et al*., 2001; Solar and Brown, 2001;).

7. Discussion and Metamorphic evolution

According to the petrographic study, it is proposed a metamorphic path which aims to explain the tectono-metamorphic evolution of the CMB during the Variscan Orogeny.

In short, the most penetrative structure found in the Douro Group metasedimentary rocks corresponds to S_2 foliation. Due to this, it is very difficult to constrain the metamorphic prograde path, which took place during the D_1. However, the mineral assemblage in these rocks, show that attained high amphibolite metamorphic facies (sillimanite zone) during D_2.

The stromatic banded observed in metatexites with leucosomes disposed concordantly to S_2 foliation, indicates that partial melting conditions are reached during D_2. Based on the absent of primary muscovite and the abundance of biotite and sillimanite in the mesosomes, the partial melting was controlled by the following muscovite dehydration reactions, under anhydrous conditions (Thompson, 1982; Le Breton and Thompson, 1988; Patiño Douce and Harris, 1998):

Ms + Qz → Kfs + Sil + *melt* (reaction 1)
Ms + Qz + Pl → Kfs + Sil + *melt* (reaction 2)

This mineral assemblage together with the absent of garnet in the mesosomes can indicate that they didn´t attain temperature enough to the biotite dehydration, defined by following reaction (Le Breton and Thompson 1988; Vielzeuf *and* Holloway, 1988; Johannes and Holtz, 1996):

Bt + Qz + Pl + Als → Grt + Kfs + *melt*(reaction 3)

The leucosomes hosted in the mesosomes exhibit petrographic evidences that they are not in situ. Most of the leucosomes and leucogranites hosted in BMC show evidences that they resulted from partial melting of metasediments positioned in depth. The peritectic garnet in some of these igneous rocks, indicates that

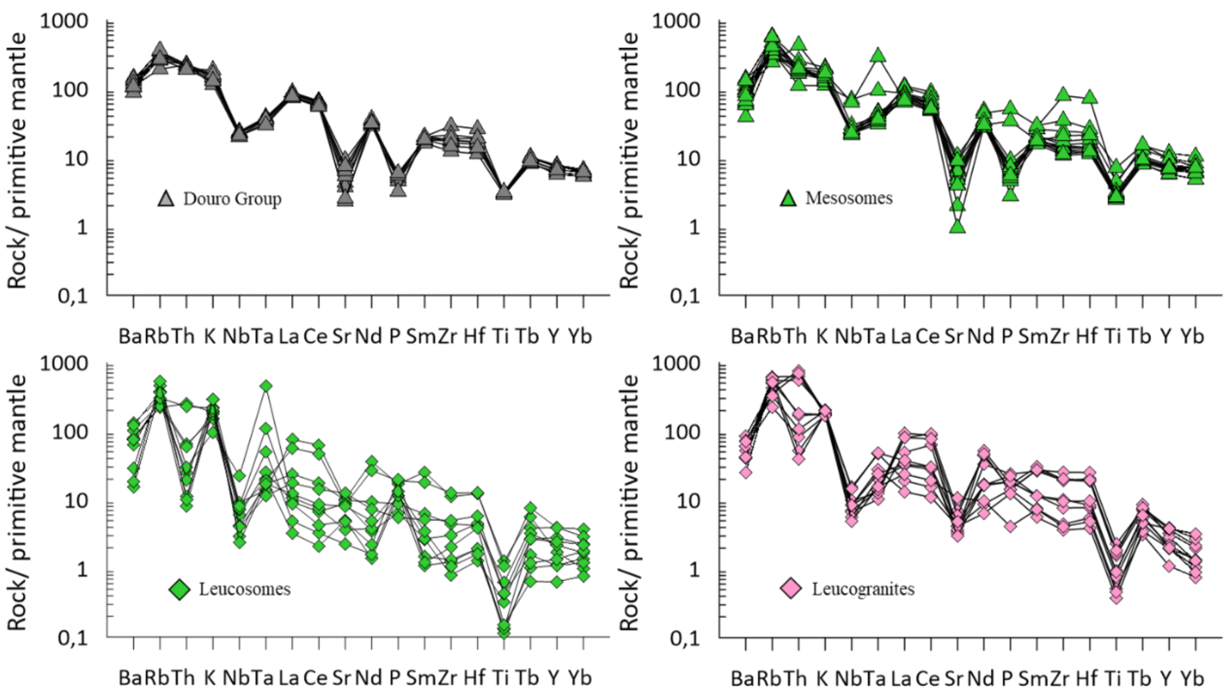

Figure 7. Multi-element diagrams normalized to primitive mantle values of Sun and McDonough (1989).
Figura 7. diagramas multielementares normalizados para os valores do manto primitive (Sun and McDonough, 1989).

precursor melts should have a deep origin and derived from biotite dehydration reaction (reaction 3).

After reaching the partial melting conditions (metamorphic peak), the rocks followed the decompression path derived by the extensional deformation (post-peak decompression stage), persisting the partial melting conditions. The decompression is responsible by the ascent and consequent injection of the melts in the BMC.

After the decompression event, already during D_3, the rocks follow a cooling path, marked by reversal reactions and the crystallization of the anatectic melts. The injected melts hosted in the BMC crystalize like leucosome veins and leucogranite sills.

In an attempt to summarize the processes and factors that controlled the geochemical heterogeneity observed in the BMC, the samples are projected in the Fe* + Mg + Ti – Na + Ca - K ternary diagram developed by Solar and Brown (2001) (Fig. 9). In this diagram were plotted the starting materials and equivalent experimental melts from Patiño Douce and Harris (1998) and Castro *et al*. (1999).

In the ternary diagram, mesosomes overlap with Douro Group metasediments and they are the samples more enriches in Fe*+Mg+Ti. Douro Group have compositions that resembling to the metapelite and metagreywacke used as starting materials in partial melting experimental studies, indicating that these rocks constitute a fertile material during anatectic event.

Leucosomes and leucogranites are plotted near to the Na+Ca - K axes, reflecting compositions dominated by quartz and feldspars. The samples are enriched in K and are projected in the

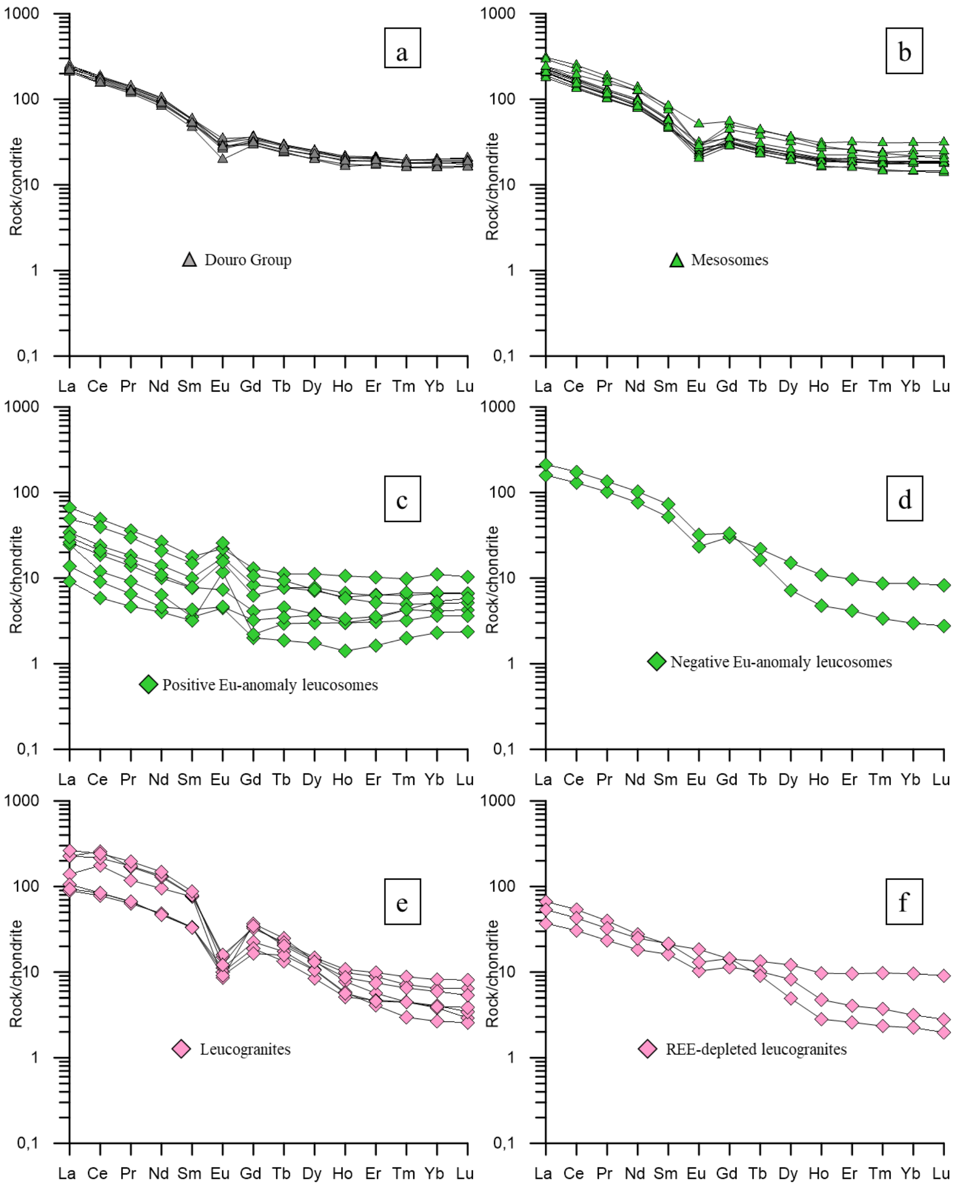

Figure 8: Rare earth diagrams normalized to chondrite values of Evensen *et al*. (1978). (a) Douro Group; (b) mesosomes; (c) leucosomes with positive Eu-anomaly; (d) leucosomes with negative Eu-anomaly; (e) leucogranites; (f) REE-depleted leucogranites.

Figura 8: Diagramas de Terras Raras normalizados para os valores do condrito (Evenson *et al*., 1978). (a) Grupo do Douro; (b) mesossomas; (c) leucossomas com anomalia positive em Eu; (d) leucossomas com anomalia negative em Eu; (e) leucogranitos; (f) leucogranitos empobrecidos em REE.

right side of the Patiño Douce *and* Harris (1998) experimental melt, in the fractionated melt field. Despite some variability found in the igneous samples, all of them are plotted in the field of fractionated melts, indicating that injected leucosomes veins and leucogranites in the BMC no longer represent original compositions. Overall, the compositional spectre observed indicates that melts already had undergone magmatic differentiation before intruding the BMC.

Most leucosomes have cummulatic composition (REE pattern with positive Eu-anomaly) indicating crystallization and removal of K-feldspar from already fractionated melts (Morfin *et al*., 2014). These samples are plotted along to the Na+Ca-K axes and reflecting different degrees of K-Feldspar accumulation.

The samples with no effects of accumulation are represented by two leucosomes and the leucogranites. They show less variability along the Na+Ca-K axis and describe a trend towards the Fe*+Mg+Ti extremitv. These rocks should have resulted from fractionated melts with different concentration/retention of residual minerals phases, as it was suggested by the REE diagrams and Spider diagrams. There is an exception to the group of leucogranites with lower REE and Zr contents. Among leucogranites, these samples have the lowest Fe*+Mg+Ti content, which indicate that rocks crystallized from melts depleted in residual mineral phases.

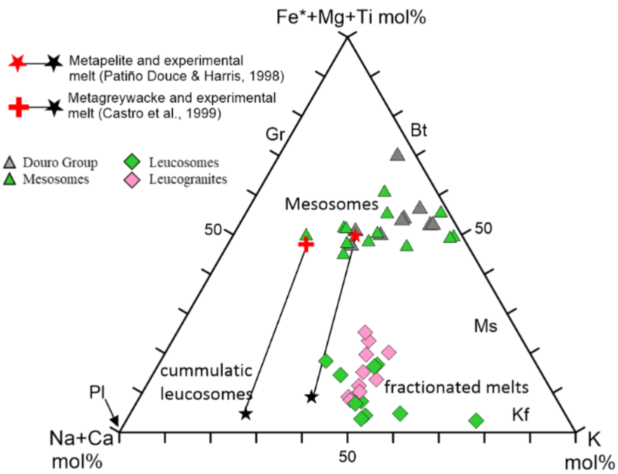

Figure 9: Projection of analysed rocks in the Molar Fe+ Mg + Ti–Na + Ca–K ternary diagram developed by Solar *and* Brown (2001). The red star symbol represents metapelite composition used as starting material in the Patiño Douce and Harris (1998) experiment, whereas red cross symbol represents metagreywacke used as starting material in the Castro *et al.* (1999) experiment. Bt = biotite; Gr = Garnet; Kf = K-feldspar; Ms = muscovite.

Figura 9: Projeção das amostras no Diagrama ternário Fe+ Mg + Ti–Na + Ca–K desenvolvido por Solar *and* Brown (2001). O símbolo com a estrela vermela representa a composição de um metapelito usado nos experimentos de fusão por Patiño Douce and Harris (1998), enquanto que o símbolo da cruz vermelha representa a composição de um metagrauvaque usado nos experimentos de fusão por Castro *et al.* (1999). Bt = biotite; Gr = granada; Kf = feldspato potássico; Ms = moscovite.

8. Conclusions

Based on field relations, petrographical and geochemical data presented in this study, it is possible to draw the following conclusions:

The Bemposta Migmatitic Complex represents a high-grade metamorphic belt, mainly composed by Douro Group metasediments that were undergone partial melting during variscan extensional deformation (D_2). The CMB was abundantly intruded by syn-tardi-D_2 leucogranites.

The metamorphic paragenesis identified in the mesosomes (particularly the abundance of biotite and sillimanite and the absence of primary muscovite and garnet) indicates that partial melting of them was controlled by muscovite dehydration reaction.

However, the stromatic leucosomes and leucogranites show evidences that mostly precursor melts resulted from anatexis of metasedimentary rocks through biotite-dehydration reactions, at a deeper structural level. After to reach the partial melting conditions, the extensional deformation induced the decompression stage, where should have persisted the anatexis conditions. The decompression stage also promoted the ascent and migration of the melts towards the BMC. During D_3, the rocks followed a cooling path, marked by retrograde reactions and the crystallization of melts. The injected melts hosted in the BMC crystalize like leucosome veins and leucogranite sills.

The geochemical data evidences the involvement of Douro Group metasediments in the anatexis event and show that this unit to be among the source materials for the Variscan granites in the CIZ (*e.g.* Azevedo *et al*., 2005; Beetsma, 1995; Neiva and Gomes, 2001; Teixeira, 2008; Valle Aguado *et al*., 2005; Villaseca *et al*., 2008).

The geochemistry also reveals that leucosomes and leucogranites no longer corresponding to the original melt compositions. They show evidence that during melt migration, they underwent fractional crystallization and accumulation of K-feldspar. Some samples also evidence retention of residual minerals, indicating higher degrees of partial melting. Other samples, such as some leucogranites, exhibit REE and Zr depletions, suggesting that low degrees of partial melting did not allow the dilution of residual mineral phases in the anatectic melt.

Thus, the CMB is interpreted as a Migmatitic Injection Complex, where anatectic melts produced at slightly deeper levels were accumulated. During the ascent, the anatetic melts was affected by processes of magmatic differentiation and variable degrees of contamination with residual mineral phases.

Acknowledgements

This work was supported by GeoBioTec and UTAD- Polo-CGeo Research Unit. The Authors also thank the Department of Geosciences of the University of Aveiro (UA), Department of Geology of the University of Trás-os-Montes and Alto Douro (UTAD), Department of Geology of the Federal University of Ceará (UFC) and Institute of Geosciences of the University of São Paulo (USP). This study also was financed in part by the Coordenação de Aperfeiçoamento de Pessoal de Nível Superior – Brasil (CAPES).

References

Arenas, R., Gil Ibarguchi, J., González Lodeiro, F., Klein, E., Martínez Catalán, J., Ortega Gironés, E., Pablo Macía, J., Peinado, M., 1986. Tectonostratigraphic units in the complexes with mafic and related rocks of the NW of the Iberian Massif. *Hercynica*, **II**(2): 87-110.

Arenas, R., Martínez Catalán, J. R., 2003. Low-P metamorphism following a Barrovian-type evolution. Complex tectonic controls for a common transition, as deduced in the Mondoñedo thrust sheet (NW Iberian Massif). *Tectonophysics*, **365**: 143-164. https://doi.org/10.1016/S0040-1951(03)00020-9.

Ayres, M., Harris, N., 1997. REE fractionation and Nd-isotope disequilibrium during crustal anatexis: Constraints from Himalayan leucogranites. *Chemical Geology*. **139**: 249-269. https://doi.org/10.1016/S0009-2541(97)00038-7.

Azevedo, M., Valle Aguado, B., Nolan, J., Martins, M., Medina, J., 2005. Origin and emplacement of syn-orogenic Variscan granitoids in Iberia the Beiras massif. *In*: Carosi, R., Dias, R., Iacopini, D., Rosenbaum, G. (Eds.), *The Southern Variscan Belt, Journal of the Virtual Explorer*, Electronic Edition, **19**(7): 18.

Barker, F., 1979. Trondhjemite: definition, environment and hypotheses of origin. *In*: Barker, F. (Ed.), *Trondhjemites, Dacites and Related Rocks*. Developments in Petrology, Elsevier, Amsterdam, **6**: 1-12.

Bea, F., Pereira, M. D., Stroh, A., 1994. Mineral/leucosome trace-element partitioning in a peraluminous migmatite (a laser ablation-ICP-MS study). *Chemical Geology*, **117**: 291-312. https://doi.org/10.1016/0009-2541(94)90133-3.

Bea, F., 1996. Residence of REE, Y, Th and U in granites and crustal protoliths; Implications for the chemistry of crustal melts. *Journal of Petrology*, **37**: 521-552. https://doi.org/10.1093/petrology/37.3.521.

Bea, F, Montero, P, Talavera, C, Zinger, T., 2006. A revised Ordovician age for the oldest magmatism of Central Iberia: U–Pb ion microprobe and LA-ICPMS dating of the Miranda do Douro orthogneiss. *Geologica Acta*, **4**: 395-401. https://doi.org/10.1344/105.000000353.

Beetsma, J. J., 1995. *The Late Proterozoic/Paleozoic and Hercynian Crustal Evolution of the Iberian Massif, N Portugal.* (Ph.D. Thesis) Vrije University, Netherlands, 223.

Behr, H. J., Engel, W., Franke, W., Giese, P., Weber, K., 1984. The Variscan belt in central Europe: Main structures, geodynamic implications, open questions. *Tectonophysics*, **109**: 15-40.

Brown, M., 2002. Retrograde processes in migmatites and granulites revisited. *Journal of Metamorphic Geology*, **20**: 25-40.

Castro, A., Patiño Douce, A. E., Corretgé, L. G., De la Rosa, J. D., El-Biad, M., El-Himidi, H., 1999. Origin of peraluminous granites and granodiorites, Iberian massif, Spain: an experimental test of granite petrogenesis. *Contributions to Mineralogy and Petrology*, **135**: 255-276. https://doi.org/10.1007/s004100050511.

Castro, A., Guillermo Corretgé, L. Mohammed El-Biad, M., El-Hmidi, H., Fernández, C., Patiño Douce, A. E., 2000. Experimental Constraints on Hercynian Anatexis in the Iberian Massif, Spain. *Journal of Petrology*, **41**(10): 1471-1488, https://doi.org/10.1093/petrology/41.10.1471.

Dias da Silva, I., 2013. *Geología de las Zonas Centro Ibérica Y Galicia–Trás–Os-Montes en la parte oriental del Complejo De Morais, Portugal/España*. Tese de Doutoramento. Universidad de Salamanca, 391.

Dias, R., Ribeiro, A., 1995. The Ibero-Armorican Arc: a collisional effect against an irregular continent? *Tectonophysics*, **246**: 13-128. https://doi.org/10.1016/0040-1951(94)00253-6.

Dias, R., Coke, C., Ribeiro, A., 2006. Da deformação da Serra do Marão ao zonamento do autóctone da Zona Centro-Ibérica. *In*: Dias, R., Araújo, A., Terrinha, P., Kullberg, J. C. (Eds.), *Geologia de Portugal no contexto da Ibéria*, Évora, Universidade de Évora, 35-61.

Dias, R., Ribeiro, A., Coke, C., Pereira, E., Rodrigues, J., Castro, P., Moreira, N., Rebelo, J., 2013. Evolução estrutural dos sectores setentrionais do autóctone da Zona Centro-Ibérica. *In*: Dias, R., Araújo, A., Terrinha, P., Kullberg, J. C. (Eds.), *Geologia de Portugal, Volume I – Geologia Pré-mesozóica de Portugal*, Escolar Editora, 73-147.

Dias, R., Ribeiro, A., Romão, J., Coke, C., Moreira, N., 2016. A review of the arcuate structures in the Iberian Variscides; constraints and genetical models, *Tectonophysics*, **681**: 170-194. https://doi.org/10.1016/j.tecto.2016.04.011.

Díez Balda, M. A., Vegas, R., González Lodeiro, F., 1990. Central Iberian Zone: Structure. *In*: Dallmeyer, R. D., Martínez García, E. (Eds.), *Pre-Mesozoic Geology of Iberia*. Springer, Berlin Heidelberg, 172-188.

Ellis, D. J., Obata, M., 1992. Migmatite and melt segregation at Cooma, New South Wales. *Trans. R. Soc. Edinburgh: Earth Sci*, **83**: 95-106. https://doi.org/10.1130/SPE272-p95.

Escuder Viruete, J., Arenas, R., Martínez Catalán, J. R., 1994. Tectonothermal evolution associated with Variscan crustal extension in the Tormes Gneiss Dome (NW Salamanca, Iberian Massif, Spain). *Tectonophysics*, **238**: 117-138. https://doi.org/10.1016/0040-1951(94)90052-3.

Escuder Viruete, J., Indares, A., Arenas, R., 1997. P–T path determinations in the Tormes Gneissic Dome, NW Iberian Massif, Spain. *Journal of Metamorphic Geology*, **15**: 645-663. https://doi.org/10.1111/j.1525-1314.1997.tb00641.x.

Escuder Viruete, J., Hernáiz Huerta, P. P., Valverde-Vaquero, P., Rodríguez Fernández, R., Dunning, G., 1998. Variscan syncollisional extension in the Iberian Massif: structural, metamorphic and geochronological evidence from the Somosierra sector of the Sierra de Guadarrama (Central Iberian Zone, Spain). *Tectonophysics*, **290**: 87-109. https://doi.org/10.1016/S0040-1951(98)00014-6.

Escuder Viruete, J., Lindares, A., Arenas, R., 2000. P-T Paths Derived from Garnet Growth Zoning in an Extensional Setting: an example from the Tormes Gneiss Dome (Iberian Massif, Spain). *Journal of Petrology*, **41**(10): 1489-1515. https://doi.org/10.1093/petrology/41.10.1489.

Evensen, N. M., Hamilton, P. J., O'Nions, R. K., 1978. Rare-earth abundances in chondritic meteorites. *Geochimica et Cosmochimica Acta*, **42**(8): 1199-1212. https://doi.org/10.1016/0016-7037(78)90114-X.

Johannes, W., Holtz, F., 1996. *Petrogenesis and experimental petrology of granitic rocks.* Springer, Berlin. 335.

Johannes, W., Ehlers, C., Kriegsman, L. M., Mengel, K., 2003. The link between migmatites and S-type granites in the Turku area, southern Finland. *Lithos*, **68**(3-4): 69-90. https://doi.org/10.1016/S0024-4937(03)00032-X.

Julivert, M., Fontboté, J. M., Ribeiro, A., Conde, L., 1972. *Mapa Tectónico de la Península Ibérica y Baleares E. 1: 1 000 000*. Instituto Geológico y Minero de España, Madrid.

Julivert, M., Fontboté, J. M., Ribeiro, A., Conde, L., 1974. *Memória explicativa do Mapa Tectónico de la Peninsula Ibérica y Baleares (1: 1 000 000).* Instituto Geológico y Minero de España, Madrid, 113.

Lazuen Alcón, F. J., Roldán Torres, R., Gabaldón López, V., 1981. *Mapa geológico de España, escala 50.000*. Instituto Geológico y Minero de España, Hoja 395. Zamora. Muga de Sayago.

Le Breton, N., Thompson, A. B., 1988. Fluid-absent (dehydration) melting of biotite in metapelites in the early stages of crustal anatexis. *Contributions to Mineralogy and Petrology*, **99**: 226-237. https://doi.org/10.1007/BF00371463.

Leitch, A. M., Weinberg, R. F., 2002. Modelling granite migration by mesoscale pervasive flow. *Earth and Planetary Science Letters*, **200**: 131-146. https://doi.org/10.1016/S0012-821X(02)00596-4.

Martínez Catalán, J. R., Fernández-Suárez, J., Jenner, G. A., Belousova, E., Díez Montes, A., 2004. Provenance constraints from detrital zircon U–Pb ages in the NW Iberian Massif: implications for Paleozoic plate configuration and Variscan evolution. *Journal of the Geological Society*, London, **161**: 461-473. https://doi.org/10.1144/0016-764903-054.

Martínez Catalán, J. R., Arenas, R., García, F. D, Cuadra, P. G., Gómez-Barreiro, J., Abati, J., Castiñeiras, P., Fernández-Suárez, J., Martínez, S. S., Andonaegui, P. Clavijo, E. G., Montes, A. D., Pascual, F. J. R., Valle Aguado, B., 2007. Space and time in the tectonic evolution of the northwestern Iberian Massif. Implications for the Variscan belt. *In*: Hatcher, R. D., Jr., Carlson, M. P., McBride, J. H., Martínez Catalán, J. R. (Eds.), *4-D Framework of Continental Crust*. *Geological Society of America*, Boulder, Memoirs, **200**: 403-423. https://doi.org/10.1130/2007.1200(21).

Martínez Catalán, J. R., Arenas, R., Martínez Catalán, J. R, Arenas, J., Abati, J., Sánchez Martínez, S., Díaz García, F., Fernández Suárez, González Cuadra, J., P., Castiñeiras, P., Gómez Barreiro, J., Díez Montes, A., González Clavijo, E., Rubio Pascual, F. J., Andonaegui, P., Jeffries, T. E., Alcock, J. E., Díez Fernández, R., López Carmona, A. 2009. A rootless suture and the loss of the roots of a mountain chain: the Variscan belt of NW Iberia. *Comptes Rendus Geoscience*, **341**: 114-126. https://doi.org/10.1016/j.crte.2008.11.004.

Milord, I., Sawyer, E.W., Brown, M., 2001. Formation of diatexite migmatite and granite magma during anatexis of semi-pelitic metasedimentary rocks: an example from St. Malo, France. *Journal of Petrology*, **42**: 487-505. https://doi.org/10.1093/petrology/42.3.487.

Morfin, S., Sawyer, E. W., Bandyayera, D., 2013. Large volumes of anatecticmelt retained in granulite facies migmatites: an injection complex in northern Quebec. *Lithos*, **168-169**: 200-218. https://doi.org/10.1016/j.lithos.2013.02.007.

Morfin, S., Sawyer, E. W., Bandyayera, D., 2014. The geochemical signature of a felsic injection complex in the continental crust: Opinaca Subprovince, Quebec. *Lithos*, **196**: 339-355. https://doi.org/10.1016/j.lithos.2014.03.004.

Neiva, A. M. R., Gomes, M. E. P., 2001. Diferentes tipos de granitos e seus processos petrogenéticos: granitos Hercínicos portugueses. *Memórias Academia das Ciências de Lisboa*, ***XXXIX***: 53-95.

Noronha, F., Ramos, J. M. F., Rebelo, J. A., Ribeiro, A., Ribeiro, M. L., 1981. Essai de corrélation des phases de déformation hercyniennes dans le nord-ouest Péninsulaire. *Leidse Geologische Mededel*, **52**: 87-91.

O`Connor, J. T., 1965. A classification of quartz rich igneous rock based on feldspar ratios. *US Geological Survey*, **525B**: B79-B84.

Patiño Douce, A. E., Harris, N., 1998. Experimental constraints on Himalayan anatexis. *Journal of Petrology*, **39**: 689-710. https://doi.org/10.1093/petroj/39.4.689 .

Pereira, A. R., Pereira, M., Teixeira, M., Amaro, P., Bento dos Santos, T., Mata, J., 2017. Migmatitos: características petrológicas e geoquímicas, formação e evolução. *Geonovas*, **30**: 79-86.

Pereira, E., Ribeiro, A., Marques, F., Munhá, J., Castro, P., Ribeiro, M. L., Pereira, D., Noronha, F., Ferreira, N., 2001. *Carta Geológica de Portugal na escala 1:200.000, Folha 2 – Trás os Montes*. Serviços Geológicos de Portugal.

Pereira, E., Pereira, D. Í., Rodrigues, J. F., Ribeiro, A., Noronha, F., Ferreira, N., Sá, C. M., Farinha Ramos, J., Moreira, A., Oliveira, A. F. 2006. *Notícia Explicativa da Folha 2 da Carta Geológica de Portugal na escala 1:200.000*. Instituto Nacional de Engenharia, Tecnologia e Inovação, Lisboa, 119.

Ribeiro A., Munhá J., Dias R., Mateus A., Pereira E., Ribeiro L., Fonseca P., Araújo A., Oliveira T., Romão J., Chaminé H., Coke C., Pedro J., 2007. Geodynamic evolution of SW Europe Variscides. *Tectonics*, **26**: 1-24. https://doi.org/10.1029/2006TC002058 .

Ribeiro, A., Quesada, C., Dallmeyer, R. D., 1990. Geodynamic evolution of the Iberian Massif. *In*: Dallmeyer, R. D., Martínez-Garcia, E. (Eds.). *Pre-Mesozoic Geology of Iberia*, Springer-Verlag, Berlin Heidelberg, 397-410.

Sanz Santos, M. A., Carrasco González, R. M., Rubio Pascual, J. F., Martín-Serrano García, A., Rodríguez Fernández, L. R., Escuder Viruete, J., Villar Alonso, P., Díez Montes, A., Fernández Ruiz, J., 2000a. *Mapa Geológico De España, Escala 50.000*. Instituto Geológico y Minero de España, Hoja 423. Zamora. Fermoselle.

Sanz Santos, M. A., Carrasco González, R. M., Rubio Pascual, J. F., Martín-Serrano García, A., Rodríguez Fernández, L. R., Escuder Viruete, J., Díez Montes, A., 2000b. *Mapa Geológico de España, Escala 50.000, Hoja 422*. Salamanca. Aldeadávila De La Ribera.

Sawyer, E. W., 2008. *Atlas of migmatites*. The Canadian Mineralogist Special Publication, NRC Research Press, Ottawa, Ontario, **9**: 371.

Solar, G. S., Brown, M., 2001. Petrogenesis of migmatites in Maine, USA: possible source of peraluminous leucogranite in plutons?. *Journal of Petrology*, **42**: 789-823. https://doi.org/10.1093/petrology/42.4.789.

Sun, S., McDonough, W. F., 1989. Chemical and isotopic systematics of oceanic basalts: implications for mantle composition and processes. *In*: Saunders, A. D., Norry, M. J. (Eds.), *Magmatism in the Ocean Basins*. Geological Society London, Special Publication, London, **42**: 313-345.

Talavera, C., Montero, P., Bea, F., González Lodeiro F., Whitehouse, M., 2013. U-Pb zircon geochronology of the Cambro-Ordovician metagranites and metavolcanic rocks of central and NW Iberia. *Int J Earth Sci*, **102**: 1-23. https://doi.org/10.1007/s00531-012-0788-x.

Teixeira, R. S. T., 2008. *Mineralogia, petrologia e geoquímica dos granitos e seus encraves da região de Carrazeda de Ansiães*. (PhD Thesis), Universidade de Trás-os-Montes e Alto Douro, Portugal, 427.

Thompson, A. B., 1982. Dehydration melting of pelitic rocks and the generation of H_2O undersaturated granitic liquids. *American Journal of Science*, **282**: 1567-1595. https://doi.org/10.2475/ajs.282.10.1567.

Valle Aguado, B., Azevedo, M. R., Schaltegger, U., Martínez Catalán, J. R., Nolan, J., 2005. U–Pb zircon and monazite geochronology of Variscan magmatism related to syn-convergence extension in Central Northern Portugal. *Lithos*, **82**: 169-184. https://doi.org/10.1016/j.lithos.2004.12.012.

Vielzeuf, D., Holloway, J. R., 1988. Experimental determination of the fluid-absent melting relations in the pelitic system. Consequences for crustal differentiation. *Contributions to Mineralogy and Petrology*, **98**: 257-276. https://doi.org/10.1007/BF00375178.

Villaseca, C., Pérez-Soba, C., Merino, E., Orejana, D., López-García, J.A., Billstrom, K., 2008. Contrasting crustal sources for peraluminous granites of the segmented Montes de Toledo Batholith (Iberian Variscan Belt). *Journal of Geosciences*, **53**: 263-280. http://doi.org/10.3190/jgeosci.035.

Watt, G. R., Harley, S. L., 1993. Accessory phase controls on the geochemistry of crustal melts and restites produced during water-undersaturated partial melting. *Contributions to Mineralogy and Petrology*, **114**: 550-556. https://doi.org/10.1007/BF00321759.

Zeck, H. P., Wingate, M. T. D., Pooley, G., 2007. Ion microprobe U–Pb zircon geochronology of a late tectonicgranitic-gabbroic rock complex within the Hercynian Iberian belt. *Geological Magazine*, **144**: 157-177. https://doi.org/10.1017/S0016756806002652.